DEVELOPMENT AND INVESTIGATION OF INORGANIC AND ORGANIC SMART SURFACES FOR ANTI-BIOFOULING APPLICATIONS

A MASTER'S THESIS

in

Manufacturing Engineering

Atilim University

by

CANSU ERGENE

JULY 2014

DEVELOPMENT AND INVESTIGATION OF INORGANIC AND ORGANIC SMART SURFACES FOR ANTI-BIOFOULING APPLICATIONS

A THESIS SUBMITTED TO

THE GRADUATE SCHOOL OF NATURAL AND APPLIED SCIENCES

OF

ATILIM UNIVERSITY

BY

CANSU ERGENE

IN PARTIAL FULFILLMENT OF THE REQUIREMENTS FOR THE DEGREE OF

MASTER OF SCIENCE OF PHILOSOPHY

IN

THE DEPARTMENT OF MANUFACTURING ENGINEERING

JULY 2014

Approval of the Graduate School of Natural and Applied Sciences, Atılım University.

____

Prof. Dr. İbrahim Akman

Director

I certify that this thesis satisfies all the requirements as a thesis for the degree of Master of Science.

____

Prof. Dr. Engin Sadık Kılıç

Head of Department

This is to certify that we have read the thesis "DEVELOPMENT AND INVESTIGATION OF INORGANIC AND ORGANIC SMART SURFACES FOR ANTI-BIOFOULING APPLICATIONS" submitted by "Cansu Ergene" and that in our opinion it is fully adequate, in scope and quality, as a thesis for the degree of Master of Science.

______________________	______________________
Prof. Dr. Bilgin Kaftanoğlu	Asst. Prof. Dr. C. Merih Şengönül
Co-Supervisor	Supervisor

Examining Committee Members

Asst. Prof. Dr. C. Merih Şengönül	______________________
Prof. Dr. Bilgin Kaftanoğlu	______________________
Assoc. Prof. Dr. Hakan Argeşo	______________________
Asst. Prof. Dr. Caner Şimşir	______________________
Asst. Prof. Dr. Seha Tirkeş	______________________

Date: (04.07.2014)

I declare and guarantee that all data, knowledge and information in this document has been obtained, processed and presented in accordance with academic rules and ethical conduct. Based on these rules and conduct, I have fully cited and referenced all material and results that are not original to this work.

Name, Last name: Cansu Ergene

Signature:

ABSTRACT

DEVELOPMENT AND INVESTIGATION OF INORGANIC AND ORGANIC SMART SURFACES FOR ANTI-BIOFOULING APPLICATIONS

Ergene, Cansu

M.S., Manufacturing Engineering Department

Supervisor: Asst. Prof. Dr. C. Merih Şengönül

Co-Supervisor: Prof. Dr. Bilgin Kaftanoğlu

July 2014, 79 pages

Biofilm formation on medical devices particularly during long-term use is the cause of many hospital-acquired infections. Most of the time, they extend the healing process and bring about high medical expenditures due to perpetual complications. To modify surfaces in a way resistant to bacterial adhesion could be a powerful approach to combat biofilm formation. In the context of this thesis, we aimed to develop inorganic and organic smart surfaces for anti-biofouling applications. First, we studied on the bacteriostatic effect of boron nitride (BN) coatings with c-BN and h-BN like crystallographic structures on AISI 316L steel. Here we report how the spatial arrangement of atoms affected the bacterial accumulation on specimen surfaces. Furthermore, for the case of organic surfaces, we investigated the antibacterial behavior of silicone rubber surfaces modified by immobilized cationic peptide, Lactoferricin B (LFB). In this research, we observed successful conjugation of a peptide and its lethal action on *S. epidermidis* and *P. aeruginosa*, generally encountered microorganisms which develop biofilm on catheters

Keywords: Biofilm, bacterial adhesion, anti-biofouling, bacteriostatic, bactericidal, boron nitride (BN), cationic peptide, Lactoferricin B (LFB)

ÖZ

MİKROORGANİZMALARIN YAPIŞMASINI ÖNLEYİCİ İNORGANİK VE ORGANİK AKILLI YÜZEYLERİN GELİŞTİRİLMESİ VE İNCELENMESİ

Ergene, Cansu

Yüksek Lisans, İmalat Mühendisliği Bölümü

Tez Yöneticisi: Yrd. Doç. Dr. C. Merih Şengönül

Ortak Tez Yöneticisi: Prof. Dr. Bilgin Kaftanoğlu

Temmuz 2014, 79 sayfa

Özellikle uzun süreli kullanımları sırasında tıbbi cihazların yüzeyinde meydana gelen biyofilm oluşumu, hastane ortamında yakalanılan birçok enfeksiyonun temel nedenidir. Çoğu zaman bu enfeksiyonlar, iyileşme sürecini gecikmeye uğratmakta ve sürekli kendisini tekrarlayabilen komplikasyonlar sonucu maliyeti yüksek müdahalelere sebep olmaktadır. Bakteri yapışmasına dirençli yüzeyler hazırlamak, biyofilm oluşumuyla mücadelede etkili bir yaklaşım olabilir. Bu tez çalışmasıyla, mikroorganizmaların yüzeye yapışmasını engelleyici inorganik ve organik akıllı yüzeyler geliştirilmesi hedeflenmiştir. İlk olarak, AISI 316L çelikleri üzerinde kubik ve hekzagonal benzeri kristalografik yapılarda bulunan bor nitrür (BN) kaplamaların bakteriyostatik davranışı incelenmiştir. Bu çalışmada, atomların kristalografik düzenlerinin bakteri yapışmasına etkisi ortaya konmuştur. Organik yüzey çalışmasında ise, katyonik peptit, Laktoferisin B (LFB)'nin kimyasal olarak bağlanmasıyla modifiye edilmiş silikon kauçuğu yüzeylerin antibakteriyel aktiviteleri değerlendirilmiştir. Bu çalışma sonucunda, peptitlerin yüzeye başarılı bir şekilde bağlandıkları ve kataterlerde genellikle biyofilm oluşumuna yol açan *S. Epidermidis* ve *P. aeruginosa* gibi bakterilere karşı öldürücü etkileri gözlemlenmiştir.

Anahtar Kelimeler: Biyofilm, bakteri yapışması, biyolojik kirlilik önleyici, bakteriyostatik, bakteri öldürücü, bor nitrür (BN), katyonik peptit, Laktoferisin B (LFB)

To My Family

ACKNOWLEDGMENTS

I express sincere appreciation to my supervisor Asst. Prof. Dr. C. Merih Şengönül for his guidance, encouragement, and insight throughout the research. I could not achieve my future goals without his valuable contributions. In addition, I would like to thank my co-supervisor Prof. Dr. Bilgin Kaftanoğlu for his continuous support.

I am so grateful to Dr. Derya Biriken for her countless contributions, and patience. Thanks also go to National Boron Research Institute (BOREN) for their support. Especially, I thank to Nihan Dökmetaş and Hakan Kalkan for their sincere friendship and help. Technical assistance of Metal Forming Center of Excellence is also gratefully acknowledged.

I express my gratitude to the department of Chemical Engineering and Applied Chemistry of Atilim University and Medical Microbiology department of Ankara University.

I would like to thank Prof. Dr. Mehmet Uğur for confocal microscopy imaging. I am also thankful to Hilal Gözler and Nanomagnetics Instruments for AFM measurements.

Throughout my postgraduate education, for their presence and encouragement, I thank to my family. Finally, I offer sincere thanks to my hero, Volkan Emren for his limitless energy and patience during this period.

TABLE OF CONTENTS

LIST OF FIGURES

FIGURES

LIST OF TABLES

TABLE

LIST OF ABBREVIATIONS

3D	-	Three-dimensional
AFM	-	Atomic Force Microscopy
Ag	-	Silver
AMP	-	Antimicrobial Peptide
Ar	-	Argon
Arg	-	Arginine
As-rec	-	As-received
ATR	-	Attenuated Total Reflectance
BHI	-	Brain Heart Infusion
BN	-	Boron Nitride
BSE	-	Backscattered Electron
C	-	Carbon
C=O	-	Carbonyl
Ca	-	Calcium
c-BN	-	Cubic Boron Nitride
CEST	-	Carboxyethylsilanetriol
CFU	-	Colony Forming Unit
Cu	-	Copper

Cys	-	Cystine
EDC	-	1-Ethyl-3-(3-dimethylaminopropyl) carbodiimide
EMB	-	Eosin Methylene Blue
FTIR	-	Fourier Transformed Infrared
GaAs	-	Gallium Arsenide
Ge	-	Germanium
H	-	Hydrogen
HA	-	Hyaluronic Acid
h-BN	-	Hexagonal Boron Nitride
HCl	-	Hydrochloric Acid
IR	-	Infrared
IVC	-	Intravascular Catheter
KBr	-	Potassium Bromide
LaB_6	-	Lanthanum Hexaboride
LFB	-	Lactoferricin B
Lys	-	Lysine
MES	-	2-(*N*-morpholino) ethanesulfonic acid
Mg	-	Magnesium
N	-	Nitrogen
Na	-	Sodium
NaOH	-	Sodium Hydroxide

NHS	-	*N*-Hydroxysuccinimide
O	-	Oxygen
OH	-	Hydroxyl
PBS	-	Phosphate Buffered Saline
PDMS	-	Polydimethylsiloxane
PMMA	-	Polymethyl methacrylate
Pt	-	Platinum
PVD	-	Physical Vapor Deposition
RF	-	Radio Frequency
SAM	-	Self-assembled Monolayer
SE	-	Secondary Electron
SEM	-	Scanning Electron Microscopy
Si	-	Silicon
SS	-	Stainless Steel
TO	-	Transverse Optical
UC	-	Urinary Catheter
UDA	-	Undecylenic Acid
UV	-	Ultraviolet
W	-	Tungsten
WCA	-	Water Contact Angle
ZnSe	-	Zinc Selenide

NOMENCLATURE

R_a	Arithmetical Mean Roughness
θ	Contact Angle
γ	Free Energy Change
γ_{sv}	Solid-vapor Interfacial Free Energy
γ_{lv}	Liquid-vapor Interfacial Free Energy
γ_{sl}	Solid-liquid Interfacial Free Energy
γ_l^d	Dispersive Force Component of Liquid
γ_l^h	Hydrogen Bonding Component of Liquid
γ_s^d	Dispersive Force Component of Solid
γ_s^h	Hydrogen Bonding Component of Solid
M_w	Molecular Weight

CHAPTER 1

1. INTRODUCTION

1.1 Microorganisms and biofilm formation

1.1.1 Description of microorganism and microbiology

Microbiology has been described as the study of living organisms too small to be observed without magnification. Such microscopic agents are termed as microorganisms and classified into a variety of groups depending on their biological characteristics, such as bacteria, viruses, fungi, protozoa, algae, and helminthes (parasitic worms). Microbiology is a discipline of great significance that takes part in several branches of science; medicine, agricultural, aquatic and food science, ecology, genetics, biochemistry, and molecular biology i.e. [1, 2].

For years, humans have taken advantages of microorganisms in many ways to improve life and shape civilizations. One important example would be fermentation process, an indispensible technique in food industry. In spite of all these benefits they yield, unfortunately there are around 2000 different types of microbes which have threatened human health causing various infectious diseases and even sometimes devastation of societies [1, 2].

1.1.2 Cell types and their properties

Cells are classified into two groups as procaryotic and eucaryotic cells. Procaryotic cells (Fig.1a) are usually smaller and morphologically simpler than eucaryotic cells. In contrast to eucaryotes (Fig.1b), they lack membrane-bound cell structures such as nucleus and organelles which are responsible for performing specific functions within the cell. All bacteria and Achaea are procaryotes, whereas all other organisms –algae, fungi, protozoa, higher plants and animals– have eucaryotic cells [1, 2].

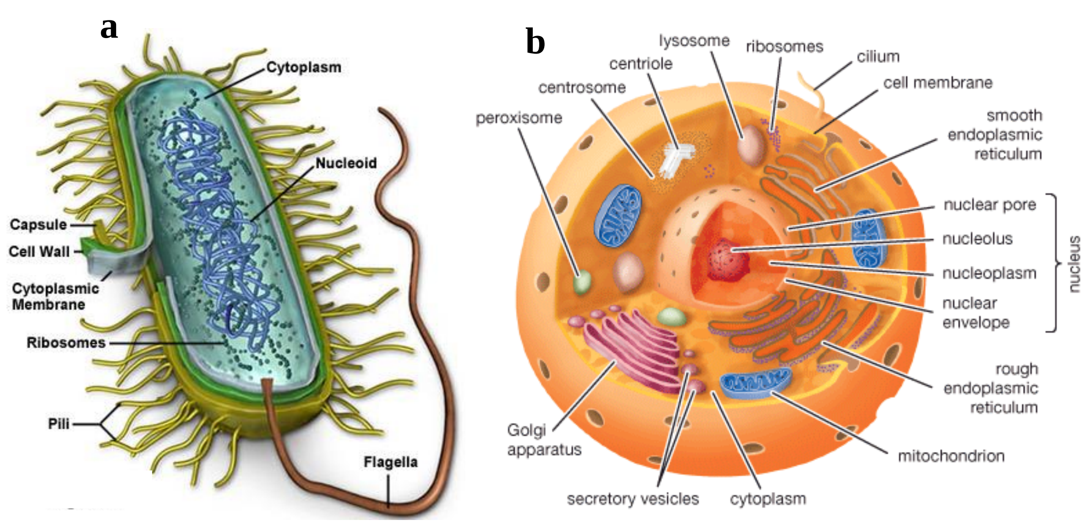

Fig. 1 Cell structure of (a) a procaryote (b) an eucaryote

Bacteria can also be categorized into two major groups according to their cell wall/membrane structure; gram-positive and gram-negative bacteria. As shown in Fig.2, gram (+) bacterium consists of thick cell wall, composed of peptidoglycan and cell membrane. For instance, *Staphylococcus epidermidis, Staphylococcus aureus, Streptococcus pneumonia, Clostridium botulinum, Bacillus subtilis, Listeria monocytogenes* are all gram (+) bacteria. *Pseudomonas aeruginosa, Escherichia coli,* *Neisseriaceae meningitis, Klebsiella pneumonia* and *Salmonella enterica* are gram (-) cells that exhibit a complete sandwich morphology with three layers: an outer layer, thin cell wall and cell membrane [1].

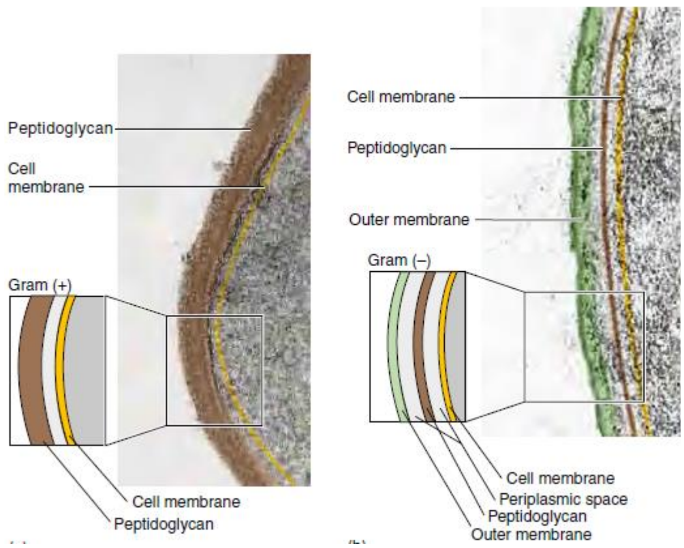

Fig. 2 Cell wall structure of gram-positive and gram-negative bacteria [1]

Furthermore, yeasts are spherical to egg shaped, unicellular microscopic fungi which involve most of the eucaryotic organelles with the exception of flagella. *Candida albicans, Crytococcus neoformans, Malassezia furfur, Coccidioides immitis, Saccharomyces cerevisiae* are some renowned instances of yeasts [1, 2].

1.1.3 Biofilm formation

Biofilm is an accumulated biomass of both bacteria and fungi, enclosed in a self-produced extracellular matrix and adherent to an inert or living surface [3-6]. Even if some biofilms have positive impacts on human health, such as organisms inhabiting the lining of a healthy intestine and the female genito-urinary tract, biofilm formation on medical devices generally causes the major complications which result with serious ailments that might even lead to death [6]. Table 1 indicates common biofilm-associated infections with contributory species.

Table 1 Human infections involving biofilm [6]

Infection or disease	Common biofilm bacterial species
Dental caries	Acidogenic Gram-positive cocci (e.g., *Streptococcus*)
Periodontitis	Gram-negative anaerobic oral bacteria
Otitis media	Nontypable strains of *Haemophilus influenzae*
Musculoskeletal infections	Gram-positive cocci (e.g., staphylococci)
Necrotizing fasciitis	Group A streptococci
Biliary tract infection	Enteric bacteria (e.g., *Escherichia coli*)
Osteomyelitis	Various bacterial and fungal species—often mixed
Bacterial prostatitis	*E. coli* and other Gram-negative bacteria
Native valve endocarditis	Viridans group streptococci
Cystic fibrosis pneumonia	*P. aeruginosa* and *Burkholderia cepacia*
Meloidosis	*Pseudomonas pseudomallei*
Nosocomial infections	
ICU pneumonia	Gram-negative rods
Sutures	*Staphylococcus epidermidis* and *S. aureus*
Exit sites	*S. epidermidis* and *S. aureus*
Arteriovenous shunts	*S. epidermidis* and *S. aureus*
Schleral buckles	Gram-positive cocci
Contact lens	*P. aeruginosa* and Gram-positive cocci
Urinary catheter cystitis	*E. coli* and other Gram-negative rods
Peritoneal dialysis (CAPD) peritonitis	A variety of bacteria and fungi
IUDs	*Actinomyces israelii* and many others
Endotracheal tubes	A variety of bacteria and fungi
Hickman catheters	*S. epidermidis* and *C. albicans*
Central venous catheters	*S. epidermidis* and others
Mechanical heart valves	*S. aureus* and *S. epidermidis*
Vascular grafts	Gram-positive cocci
Biliary stent blockage	A variety of enteric bacteria and fungi
Orthopedic devices	*S. aureus* and *S. epidermidis*
Penile prostheses	*S. aureus* and *S. epidermidis*

Biofilm development provides a protected environment for microorganisms and reduces penetration of antimicrobial agents through the extracellular matrix [5, 6]. In addition, the biofilm structure includes channels in which nutrients and oxygen can circulate and cells can transfer their genes at different regions as well as remove metabolic wastes out of the cell [4]. Their inherent resistance to antibiotics via mutation and thereof survival mechanism is at the root of many persistent and chronic microbial infections [4].

Formation of biofilm consists of four main stages:

a) Conditioning film deposition: Upon implantation of medical devices, their surface is immediately covered by bodily fluids, such as saliva, blood, urine and mucus. Likewise, most of the broths used in bacterial tests also contain similar proteins, various ions and polysaccharides. Formation of conditioning film changes the surface properties of the substrate and creates binding sites for pathogens to attach and colonize [6].
b) Initial microbial approach and attachment: Fig.3 simply represents the forces acting on bacterial adhesion with respect to the distance from the substrate surface. At the beginning, just weak van der Waals' interactions take place at distances > 50 nm where a bacterium and surface are too far for bacteria to recognize the surface. Getting closer, electrostatic repulsive forces act between the bacteria and the substrate at 10 to 20 nm from the surface. If a bacterium overcomes the barrier of electrostatic repulsion, it begins approaching towards the surface exposed to a variety of short-range chemical interactions. These time-dependent interactions could be electrostatic, hydrophobic and specific interactions where receptor-mediated adhesions do happen via bacterial surface appendages; hence, all of them result in irreversible binding to material surface [6, 7].
c) Growth and colonization: Once they attach, organisms start producing polysaccharides which envelop and provide them accommodation on the surface [6].
d) Biofilm formation: Finally, microbial colonies make up the biofilm that protects them against antibiotics and host immune defense [6].

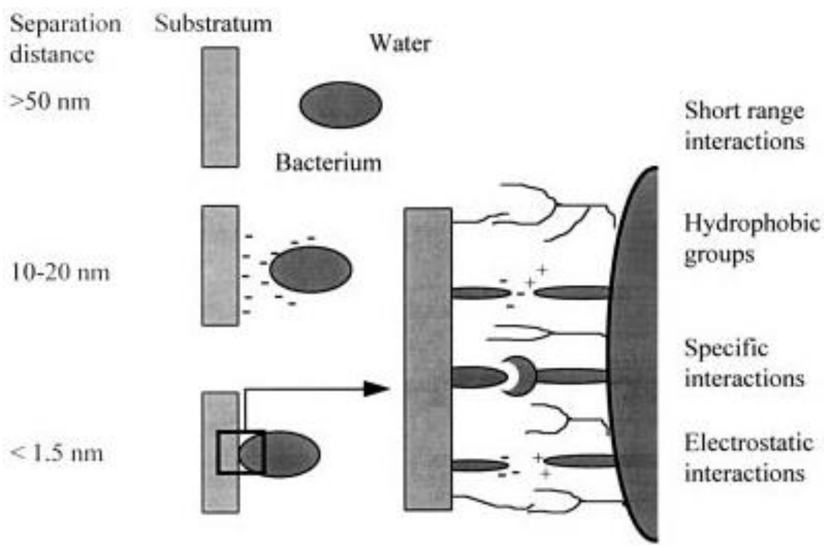

Fig. 3 The adhesion process and acting forces [8]

1.2 Antibacterial activity and its mechanism

Antibacterial activity is associated with agents which prevent bacterial adhesion and colonization, and eliminate microorganisms on substrate surfaces without any cytotoxicity to surrounding healthy tissue [8, 9]. These compounds can be divided into two groups; "bactericidal" which locally kills bacteria and "bacteriostatic" which slows down bacterial growth [9].

There are several mechanisms that destroy bacterial cells. One of them may be damage to the bacterial cytoplasmic membrane that possesses vital functions to the cell survival [10]. Disruption of bacterial membrane sometimes ends up with leakage of cellular contents, named plasmolysis [8, 10]. Some reports showed that disruption of cell wall synthesis constrains its power functions; permeability and respiration [8, 10, 11]. Third mechanism is the protein denaturation which causes the inhibition of enzyme activity and disruption of cellular metabolism [10]. Moreover, antimicrobial agents damage the DNA, hence hinders its replication. However, such an activity sometimes leads to lethal mutations [8, 10].

Bacteriostatis also plays an important role in inhibiting bacterial colonization. Especially, it suppresses the pathogens by prolonging their time of growth beyond the normal duration. Thus, it provides necessary time to natural immune defense for launching the adequate response to prevent infections [12].

1.3 Antimicrobial applications

Prevention of microbial adhesion or at least avoiding the growth of already attached or colonizing microorganisms is a great concern in plenty of medical, food and other industrial applications [5, 13]. In the last two decades, researches have mainly centered upon the modification of material surfaces with coatings made by surface adsorption and chemical grafting or impregnation of the bulk material with one or more antimicrobial compounds [5].

Cassinelli et al. showed that hydrophilic coatings can be an approach to obtain antibacterial materials. They modified PMMA intraocular lenses with hydrophilic hyaluronic acid (HA) that showed remarkable reduction in fibroblast and *S. epidermidis* adhesion [14]. Besides, John et al. studied with hydrogel-coated urethral stents which exhibited increased ability to retain and release antibiotics to targeted location [15]. Heparin coatings or bindings could be another alternative to avert microbial adhesion and colonization [16, 17]. What's more, Berendjchi and his group worked on cotton surfaces doped by silica-based sols with Cu nanoparticles and revealed perfect antibacterial effect against both gram (-) and gram (+) bacteria [18].

For centuries, it has been well-known that silver (Ag) and its ions and compounds have employed effective inhibitory and bactericidal performance against a wide range of microorganisms [19-28]. Silver links groups of enzymes and interacts with nucleic acids which lead to the cell death eventually [25, 26]. In addition, Ag accumulates in the bacterial cell wall as granules that annihilate cell division while damaging the cell envelope and cellular contents. [25, 26, 29]. Recent studies on silver have focused on its nanoparticles since silver at nanoscopic scale provides larger surface area which enhances its the antimicrobial efficacy [22, 25, 26].

Boron and boron-containing compounds are another inorganic agents which exhibit strong antibacterial activity especially against gram (-) bacteria [30, 31]. They are generally bacteriostatic and thus usually interfere with the production of a cell envelope component [30].

Antimicrobial peptides (AMPs) are such a new promising trend of antibiotics which are naturally part of the innate defense mechanism of all multicellular organisms [32-35]. Unlike other antimicrobial agents, these peptides can be attained by simple isolation from various species of animals, plants, bacteria, fungi and viruses [32, 34, 35]. They are positively charged due to Lys and Arg of amino acid groups (net charge of +2 to +9) and usually composed of short amino acid sequences (12-50 residues) which accommodate some amphipathic (both hydrophobic and hydrophilic) domains as well [32-35]. Though they have a high bactericidal effect against a broad spectrum of fungi, gram (+) and gram (-) bacteria and viruses, they are almost non-cytotoxic to neutrally charged mammalian cells [33, 36]. Even at low concentrations, AMPs act as a fast killing agent and do not induce bacterial resistance and mutation [32, 33]. In general, they have a tendency to interact with negatively charged microbial outer layer which provokes cell disruption ultimately [32, 33]. They are also ideal compounds to start with while designing new synthetic AMPs with increased antimicrobial performance and preserved activity when bound to a biomaterial surface [35, 36]. Defensin, magainin, indolicidin, thanatin, burofinmelittin and lactoferricin are some examples of cationic peptides used as antimicrobial compounds in recent inquiry for an alternative antimicrobial agents [34].

1.4 Scope of the thesis work

In the context of this thesis work, we aimed to develop surfaces that can resist to the adhesion of microorganisms which are notorious for their involvement in many hospital-acquired infections. For this purpose, our research study focused on smart coatings with anti-biofouling properties for metallic and polymer substrates. 316L stainless steel was chosen as metallic substrate since it is one of the most frequently used steel grade in the manufacture of surgical instruments while silicone rubber was chosen as polymer substrate regarding its increasing popularity in the catheter industry.

Likewise the coating materials were chosen according to the substrates constitution. Therefore, boron nitride (BN) which is an inorganic material was used for coating of 316L steel, whereas cationic peptide lactoferricin B (LFB) was used for silicone rubber surface modification.

Boron is an element known for its bacteriostatic effects and hence widely used in cosmetic industry. Boron nitride especially in cubic form (c-BN) is the second hardest material after diamond. Because of this property, it is utilized especially as coatings for tool and dies to increase their life span. However, to the best of our knowledge, there is no research on bacteriostatic effects of boron nitride in cubic as well as in other crystallographic forms. Because c-BN would be a good candidate for improving expensive surgical instruments against abrasion and resistance, it would be even better if somehow it provides anti-microbial properties to them. With this intention, PVD coated hexagonal and cubic like structures of BN thin films on 316 L steel were tested against *E. coli* colony formations. We explored both coatings with respect to surface roughness, surface free energy via contact angle measurements, as well as surface charge density via force-distance interactions.

On the other hand, developing anti-microbial silicone rubber surfaces was our second goal in the framework of this thesis. With this intention we decided to use a nature made antimicrobial peptide LFB obtained from protein lactoferrin. We grafted both undecylenic acid and carboxyethylsilanotriol (CEST) on silicone rubber surfaces as anchor molecules for peptide LFB. Both molecules have carboxylic acid groups as the functional terminal group dangling out from the surface. Carbodiimide (EDC) was used to activate carboxylic acid groups while N-hydroxy succinamide was used to stabilize these groups for further reaction with the amine groups in lysine residues of the LFB via nucleophilic substitution. According to ATR-FTIR data, we confirmed successful conjugation of LFB with undecylenic acid grafts. Surfaces were analyzed by confocal and scanning electron microscopy, as well as contact angle measurements. Following surface modifications, LFB coated samples were tested against *S. epidermidis* and *P. aeruginosa*.

CHAPTER 2

2. INVESTIGATION OF BORON NITRIDE (BN) THIN FILM COATINGS FOR ANTIBACTERIAL PURPOSES

2.1 Introduction

Biofilm formation on medical devices is one of the major causes of hospital-acquired infections [37]. They usually extend the period of the treatment process which might even end up with loss of the patient and inflict high medical expenditures due to perpetual complications [5, 38, 39]. Such infections generally start with microbial adhesion to medical instruments [39]. Microbial adhesion happens via a multistage mechanism leading to build-up an antibiotic/antiseptic-resistant self-assembling multi-cellular communities, called a biofilm [4, 38-41].

Biofilm formation can be influenced by many factors associated with surface such as, its chemistry, free energy, morphology, charge and roughness. Even though they all have an overall effect on adhesion dynamics of bacteria, usually strict control of couple of these parameters can be enough to attain the anti-biofouling behavior.

In search of determining the appropriate parameters to control, scientists for years were suspecting that surface roughness has a profound effect on bacterial adhesion to surfaces. Hence, quite number of researches was made in the last decade to understand how influential this effect is [42-51]. Actually, increase in surface roughness increases amount of contact area which allows more cell membrane-substrate surface interactions for bacteria to attach and colonize [46, 51]. Furthermore, rougher surfaces may involve various surface irregularities, such as pits, grooves, abrasion defects, which protect bacteria against shear forces [43]. Bollen et al. recorded no further decrease in the average number of adhered bacteria below 200 nm surface roughness, and designated this value as “the threshold R_a” [44]. The study conducted by Libera and Wu et al. who investigated the behavior of *S. epidermidis* and osteoblasts towards Ti surfaces with different surface roughness. They asserted that not only vertical depth, but also lateral characteristic of surface roughness affect cell retention [50].

One of the effective approaches to weaken or even prevent microorganism/ substratum interactions could be smart surface coatings [39, 52] which introduces mainly a different surface chemistry unfavorable for bacterial adhesion. Indeed, even slight changes in the surface chemistry of the coatings might enhance this behavior further. For example, Zhou et al. studied on amorphous hydrogenated carbon (a-C:H) and hydrogen free carbon (H-free C) films deposited on AINI 316L steel by microwave plasma. They witnessed a decrease in the quantity of *E. coli* attached to a-C:H and H-free C films of around 67 % and 85 % respectively relative to uncoated 316L surface. These results showed that antibacterial behavior of carbon film coatings is significantly affected by the presence of H which degrades chemical inertness by creating C-H polar bonds in hydrogenated amorphous carbon films [51].

On the basis of above considerations, one may expect that change in surface chemistry, might cause a change in surface energy which could affect the bacterial adhesion on surface coatings. However, according to some recent studies [38, 53-56], a consistent correlation between bacterial adhesion and surface hydrophobicity alone has not found [56]. Tang and co-workers observed less bacterial attachment on more hydrophobic surfaces [56]. Yet, the research carried out by MacKintosh et al. on a series of different polymer surfaces showed that hydrophilic surfaces substantially reduced *S. epidermidis* colonization compared to hydrophobic ones [54]. Another opinion, surface hydrophobicity could be switched by modifying the surfaces with different chemicals so that it might be concluded that it has an auxiliary effect on bacterial adhesion [55].

The surface charge of the adhered surface coating could be a significant factor in mediating bacterial adhesion too [57-61]. Predominantly, bacteria bear a negative surface charge in contact with aqueous media [58, 62, 63]. With regard to electrostatic forces between bacteria and the surface, increasing substratum surface negative charge has higher potential to decrease bacterial adhesion [58-61, 64]. As a matter of fact, Bos et al. emphasize that any microbial cell surface may include positively charged domains which might intervene the adhesion process [57].

In this present research, we explored the effect of surface charge shift triggered by different phase formations of boron nitride coatings on adhesion behavior of with *Escherichia coli*. Boron and boron-containing materials have been generally recognized as antibacterial and antifungal agents [31, 65] with no cytotoxicity upon mammalian cells [66, 67]. However, to the best of our knowledge boron nitride compounds in thin film form are not investigated for bacterial adhesion. It mostly exists in its two equilibrium polymorphs; sp^2-bonded hexagonal (h-BN) and sp^3-bonded cubic (c-BN) morphologies which are very similar to graphite and diamond allotropes of carbon [68, 69]. h-BN phase due to its layered structure has a low friction coefficient which makes it a highly sought lubricating substance particularly for high temperature applications [70]. Moreover, c-BN with its tetrahedral structure exhibits excellent mechanical and chemical properties, such as high hardness, high wear and abrasion resistance and chemical inertness even at elevated temperatures [71]. Because of their exceptional hardness, Boron nitride (BN) thin films particularly in cubic form have also been preferred as protective coatings for tribological applications such as cutting tools [71-73]. For this purpose, we deposited BN thin films via magnetron sputtering on 316L sheet steel, which is frequently used in medical implants and surgical instruments [74].

Here we report the characterization of BN coatings on stainless steel substrates and their influence on the bacterial adhesion. Surface chemistry and crystallographic structure of BN coatings were determined by ATR-FTIR. In addition, surface topography and bacterial colonies were examined under SEM, while surface roughness was measured by AFM. In this work, we also conducted contact angle measurements with deionized water and diiodomethane to explore the effect of surface hydrophobicity/hydrophilicity on bacterial adhesion and calculate surface free energy. Surface charge density was determined from force-displacement curves attained by AFM. Eventually, bacterial culture tests on BN coatings were performed with *E. coli*, one of the mostly encountered gram-negative bacteria in hospital environment causing medical device-related infections [75].

2.2 Experimental

2.2.1 Production of boron nitride (BN) coatings

Physical vapor deposition (PVD) is an atomistic deposition in which the material streams out from a solid or liquid source in the form of atoms or molecules, its vapor phase is transported through a vacuum or low pressure gaseous environment to the sample where it is formed by condensation [76, 77]. Magnetron sputtering is such a high rate deposition technique that collects electrons near the target surface, and they are circulated on a closed path on the target surface by arrangement of magnets. It poses a high flux of electrons, creating higher density plasma from which ions can be extracted to sputter the target material [76, 78].

AISI 316L steel sheet (Azim Ticaret, Turkey) of about 1 mm in thickness with 2B surface finish (cold-rolled, annealed, pickled and skin passed) was purchased as substrate material for BN film deposition. Substrates were wire-cut into dimensions of 10 mm in both length and width by electrical discharge machine (Sodick Hightech Ver. 1.0, Japan). We used some of them as-received or mirror-like polished. Prior to magnetron sputtering, all 316L substrates and sample holders of PVD system were ultrasonically cleaned in 96% ethanol bath for 7-8 min, rinsed with deionized water and then dried under pressurized air blow.

In a typical PVD coating stage (Fig.4), we attached the substrates to sample holders which can rotate via a spindle mechanism underneath. Sintered h-BN plate target was used as cathode. At the beginning, the vacuum pressure of the chamber was brought down to 2×10^{-5} Torr and after immediately Argon (Ar) plasma was applied for about 15 min under 250 W RF for cleaning purposes. Next, Nitrogen (N_2) gas was pumped into the chamber and the ratio of Ar/N_2 gases was set to 5:1 ratio. Deposition was kept going for incessant 3 h while the chamber was held under 3×10^{-3} Torr pressure. Meanwhile, h-BN target was subjected to 700 and 900 W RF magnetron power during h-BN dominant and c-BN dominant thin film deposition, respectively.

For h-BN thin film coatings, we did not put into the spindle mechanism use and deposition was performed at 200 °C system temperature with no applied bias voltage. On the contrary, the spindle system made planetary motion at 300 °C for c-BN thin film coatings while 50V bias voltage was applied to 316L substrates. The whole system was well-preserved by closed-loop chilled water system to prevent excessive heating [70, 71].

At the end of deposition processes, we classified substrates into 5 groups, indicated in Table 3.

Table 2 Experimental parameters of h-BN and c-BN thin film deposition

Parameter	**h-BN**	**c-BN**
Target plate	Sintered h-BN	Sintered h-BN
Substrate	AISI 316L steel	AISI 316L steel
Spindle motion	Static	Planetary
Deposition pressure (Torr)	$3x10^{-3}$	$3x10^{-3}$
Ar/N_2 flow ratio	5/1	5/1
Target power (W)	700	900
Substrate bias voltage (V)	0	50
Heater temperature (°C)	200	300
Deposition duration (h)	3	3

Table 3 Substrate groups

Group	Feature
As-rec SS	Uncoated as-received 316L stainless steel
Polished SS	Uncoated mirror-like polished 316L stainless steel
h-BN as-rec	Dominantly h-BN coated as-received 316L stainless steel
h-BN polished	Dominantly h-BN coated polished 316L stainless steel
c-BN lustred	Dominantly c-BN coated roughly sandblasted 316L stainless steel

Fig. 4 PVD system

2.2.2 Fourier Transformed Infrared spectroscopy (FTIR)

FTIR is a widely used technique of infrared spectroscopy that insures a precise, rapid and non-destructive analysis, in either reflection or transmission mode [79, 80]. Each different compound consists of a characteristic spatial organization of atoms so that they never display exactly the same IR spectra [80, 81]. In general, some of the IR radiation is absorbed whereas some of them is transmitted by the sample. Thus, it results in an IR spectrum displaying called fingerprint region of the sample with absorption peaks corresponding to the frequencies of vibrations between the bonds of the atoms making up the material. Therefore, IR spectroscopy can be used for the identification of unknown materials as well as direct quantification of the components in a mixture [80].

Attenuated total reflectance (ATR) is a method based on internal reflectance as shown in Fig.4 where the sample is in contact with a sensing crystal having a high and constant refractive index such as, zinc selenide (ZnSe), germanium (Ge), Silicon (Si), gallium arsenide (GaAs) and diamond [81-83].

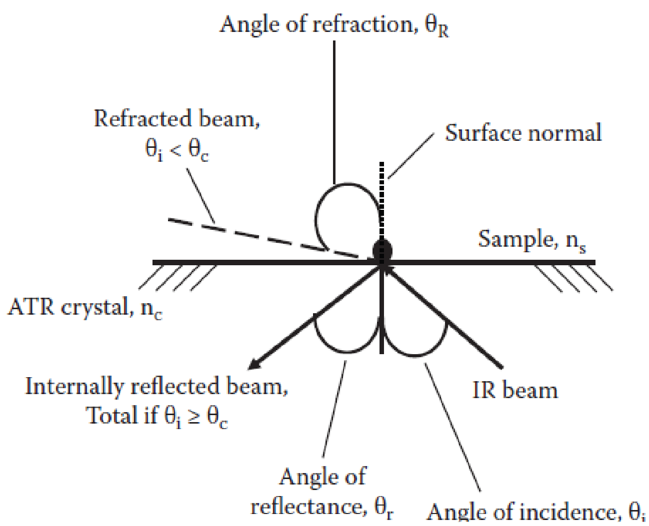

Fig. 5 Optical scheme of ATR [84]

ATR-FTIR spectroscopy (Bruker IFS55, Germany) in absorbance mode was performed to investigate the composition and crystallographic structure of BN thin film coatings. The FTIR spectra were scanned within 1700-600 cm^{-1} using a spectral resolution of 8 cm^{-1} and 32 scans. All spectra were baseline corrected, smoothed, and then peaks were fitted by mixed Gaussian-Lorentz function via spectroscopy software (Grams Suite 9.1, Thermo Fischer Scientific, PA).

2.2.3 Atomic Force Microscopy (AFM)

Atomic force microscopy (AFM) is a well-established surface topography imaging technique that provides sub-nanometer resolution in all three dimensions [84-86]. The instrument operates with a sharp tip attached to the end of the microlithographic cantilever beam that detects the substrate surface [84-86].

Fig.5 demonstrates the basic AFM set-up. Principally, AFM detects either attractive or repulsive forces between the probe tip and the surface. When the tip is repelled by or attracted to the surface, the cantilever beam deflects. The laser light senses the amplitude of the deflection and reflects from the uppermost side of the cantilever. During scanning over the surface, any vertical deflection altering the position of the laser spot on the photodetector is captured and monitored to produce a high-resolution image. AFM measurements can be conducted in air or liquids for flat surfaces but not suitable to be operated on rough or inclined surfaces [85, 86].

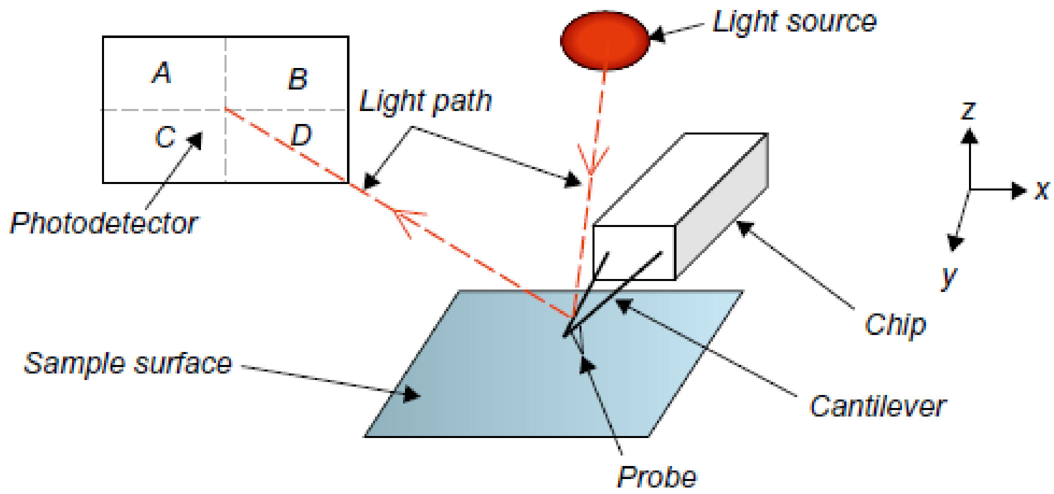

Fig. 6 Basic AFM set-up [87]

Arithmetical mean roughness (R_a) and surface topography of substrates scanned up from 77 µm x 77 µm area are determined by AFM (Nanosurf, CSM Instruments, Switzerland). Measurements in static mode were operated with a scan rate of 512 points/line in air with a silicon (Si) tip. Seven samples of each group and more than three positions per sample were imaged to analyze each substrate.

Force-displacement curves were attained in brain heart infusion (BHI) broth (Merck Millipore, Germany) by AFM (NanoMagnetics Instruments, ezAFM-Aqua, Oxford, UK) in contact mode. The cantilever and silicon nitride tip was first retracted 500 nm from the surface, then moved 1000 nm directly towards it and retracted 500 nm again. In addition, AFM (NanoMagnetics Instruments, ezAFM-Aqua, Oxford, UK) was employed in dynamic mode recorded high-resolution images of 60 µm x 60 µm area in BHI broth.

2.2.4 Scanning Electron Microscopy (SEM)

Scanning electron microscopy is the most powerful and versatile instrument to attain information about surface topography of any surface at high magnification by using a beam of highly-energetic electrons which is extracted from a W or LaB_6 filament located at the top of the gun column under high voltage [84, 87]. The beam of electrons travels under high vacuum through electromagnetic lenses that eventually focus the beam onto the sample [84]. As incident electrons impinge on a solid, electron-surface interactions take place at the top surface layer within a few nanometers to microns depth of the sample [84, 88].

Electrons in the beam are decelerated due to inelastic interactions with valance shell electrons of sample atoms which cause generation of secondary electrons as well as elastic deflections by atomic nuclei where backscattered electrons are collected from the surface [88, 89]. Within few nanometer of the surface, secondary electrons (SE) are emitted to reveal surface morphology and topography whereas backscattered electrons (BSE) emerge through an angle of more than 90° showing contrasts in composition of multiphase systems [84, 88]. Furthermore, accelerated electrons may interact with inner shell electrons to produce X-rays which is used in the chemical analysis of the surface of the sample material [88].

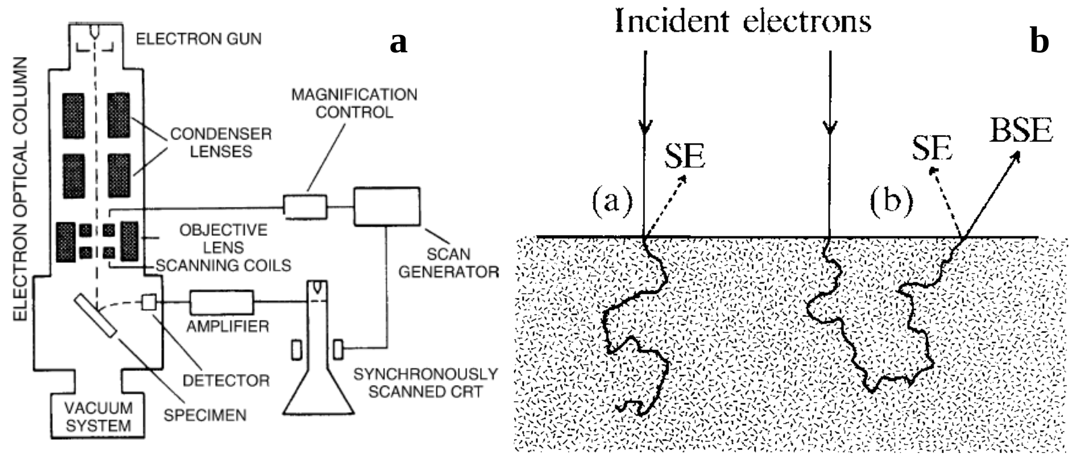

Fig. 7 Schematic diagram depicting (a) the essential parts of SEM [86] (b) production of secondary electrons (SE) and backscattered electrons (BSE) [91]

SEM (Zeiss, SmartSEM, Germany) was operated at 20 keV to visualize uncoated AISI 316L surfaces at high resolution and then voltage decreased to 10 keV for BN coated substrates in order to avoid excessive beam damage. Likewise, bacterial colonies were explored at operating voltage of 10 keV after platinum (Pt) sputtering. Images were recorded at 660-5000x magnifications with a LaB6 electron source.

2.2.5 Contact angle measurements

To investigate wetting and spreading phenomena will allow us to determine the change in surface and interfacial free energy with respect to change in various surface related factors due to change in surface constitution [90]. However, the determination of the solid-vapor (γ_{sv}) and solid-liquid (γ_{sl}) interfacial free energy is not straightforward to conduct [90]. Among the various indirect methods in measuring solid surface tensions, contact angle -purely macroscopic quantity- is the simplest and the most versatile technique [90, 91]. Thomas Young explained the mechanical equilibrium of a liquid droplet resting on a flat solid surface under the actions of three phases shown in Fig.7 [92, 93].

$$\gamma_{SV} - \gamma_{SL} = \gamma_{LV} \cos\theta$$

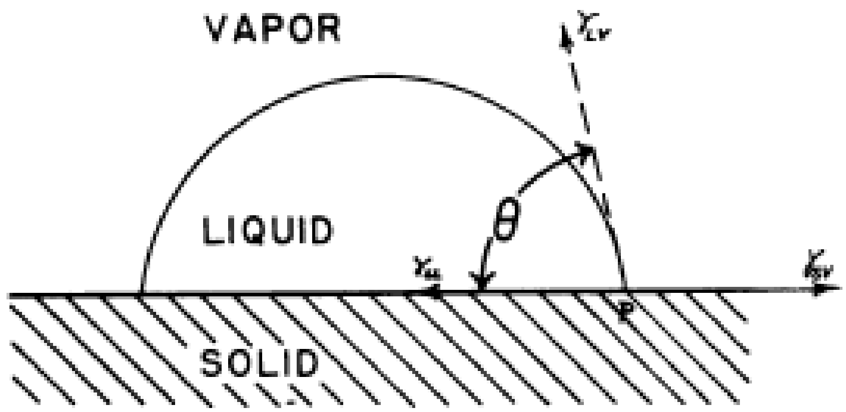

Fig. 8 Contact angle of a sessile drop [95]

Contact angle ranges between 0° and 180° according to solid-liquid interactions in an inert environment [91]. A droplet with a contact angle of 0° ($\theta = 0°$) spreads all over the solid surface while $\theta = 180°$ indicates complete non-wetting [93]. Contact angle can often vary due to the effects of chemical heterogeneity and surface roughness or texture on the same media [91].

Contact angle determinations by the sessile drop method were conducted using a tensiometer (Attension Theta Lite Optical, Finland). 2.00 μl droplet of a liquid was placed on a surface at room temperature. In total, seven samples used from each group and each sample tested with at least three drops. Each measurement took 3 s in which 36 photographs were captured. Images of drops were characterized by image processing software (OneAttension) to calculate mean contact angle.

Surface free energy reveals the free energy change γ as the surface area of a material is increased by unit area [91]. Deionized water and diiodomethane (Sigma-Aldrich, Germany) were liquid probes used to calculate surface free energy of substrates according to Owens-Wendt theory [94]. Surface free energy components of the each group were determined by following equation:

$1 + \cos\theta = 2\sqrt{\gamma_s^d}\,(\sqrt{\gamma_l^d}/\gamma_{lv}) + 2\sqrt{\gamma_s^h}\,(\sqrt{\gamma_l^h}/\gamma_{lv})$ where θ is the contact angle, γ_{lv} (total surface free energy of a liquid) is equal to sum of γ_l^d (dispersive force component) and γ_l^h (hydrogen bonding component). γ_s^d and γ_s^h are dispersive force and hydrogen bonding components of the solid substrate, respectively [94]. The dispersive (non-polar) and hydrogen (polar) component of liquid probes -deionized water and diiodomethane– are given in Table 4.

Table 4 Surface free energy components of deionized water and diidomethane [96]

Liquid	**γ_l^d (mN/m)**	**γ_l^h (mN/m)**	**γ_{lv} (mN/m)**
Deionized water	21.8	51.0	72.8
Diidomethane	50.8	0	50.8

2.2.6 Bacterial culture

Escherichia coli with its over 250 strains, is highly multifaceted gram-negative bacterium, sorting of not only harmless gut commensal but also intra- or extraintestinal pathogens which comprises well-reputed colonizers of medical devices and the major causes of persistent infections, such as protatitis, biliary tract infections, and urinary catheter cystitis [95, 96].

Bacterial suspensions were prepared with *E. coli* 075 supplied by Department of Medical Microbiology, Ankara University Medical Faculty. Bacteria were cultured in BHI broth and then seeded onto Eosin Methylene Blue (EMB) agar plate, and subsequently incubated at 37 °C to grow all night long. Next day, some of the bacterial colonies were gathered from the agar plate surface and put into Phosphate Buffered Saline (PBS). Microorganisms were harvested by centrifugation at 300 rpm for 10 min and washed three times in PBS. Later, bacterial pellets were suspended in Brain Heart Infusion (BHI) broth and stained with 0.5% trypan blue. Alive cells which could not be stained were counted on Neubauer glass slider and adjusted to approximately 10^8 Colony Forming Units (CFU)/ml in BHI [97].

2.2.7 Quantification of bacterial adhesion

All BN coated and uncoated (control) stainless steel substrates were placed in bacterial suspensions and bacterial adhesion was investigated with a static soaking method. Each sample was dipped into an *E. coli* suspension (10^8 CFU/ml in BHI) and incubated at 37 °C for 4 h. After 4 h incubation, each substrate was removed from the suspension carefully and rinsed three times with PBS to detach unbound cells. At the next stage, a sample was soaked in PBS and vortexed. Then, 50 μl of liquid was ejected to inoculate onto agar plates. Plates were put into an incubator at 37 °C over night to allow bacterial growth. Following incubation, CFU were counted and the antibacterial activity (A) of the species was calculated in accordance with the formula given below [97]:

$$\mathrm{A}(\%) = \frac{\text{mean CFU (Control sample)} - \text{mean CFU (BN coated sample)}}{\text{mean CFU (BN coated sample)}} \mathrm{x}100$$

2.3 Results and Discussion

For the purpose of understanding the effect of different polymorph formations of BN on bacterial adhesion behavior, it was essential to start initially with the characterization of crystallographic structure of BN thin films developed under different coating conditions. Hence, ATR-FTIR measurements in absorbance mode were carried out accordingly. FTIR characteristic frequencies of h-BN include an absorption band at about 760-800 cm^{-1} in transversal optical mode (TO) due to out-of-plane B-N-B bending vibrations and 1364-1400 cm^{-1} (TO) due to in-plane B-N stretching vibrations, whereas c-BN phase has a strong absorption band between 1055-1100 cm^{-1} (TO) [79, 83, 98-102].

During FTIR spectroscopy, we observed the characteristic peak of h-BN at 781 cm^{-1} as shown in Fig.8a. Additionally, a broad peak which can be seen in the same figure around wavenumber 1285 cm^{-1} was analyzed by peak-fitting method. The peak was resolved as 1390 cm^{-1}, which can be assigned to h-BN. Peak shift and broadening may sometimes occur due to the thin film formation including defects, deviations in film stoichiometry and presence of the mixed crystallographic phases in it [79]. In the case of c-BN, we witnessed the strongest peak at around 1071 cm^{-1} as demonstrated in Fig.8b which is slightly above the characteristic frequency of a single-crystal c-BN peak generally observed at around 1060 cm^{-1}. Mirkarimi et al. claimed that peak shift to higher wavenumbers is due to the compressive stresses developed during thin film deposition [79]. In the same spectra there is another peak at 1527 cm^{-1}, which might be associated with amorphous phase of BN (a-BN) [83]. Since, it is difficult to attain 100% c-BN or h-BN under PVD conditions; we decided to specify the coatings according to their major fingerprint regions under ATR-FTIR even though some transition phases happened to exist.

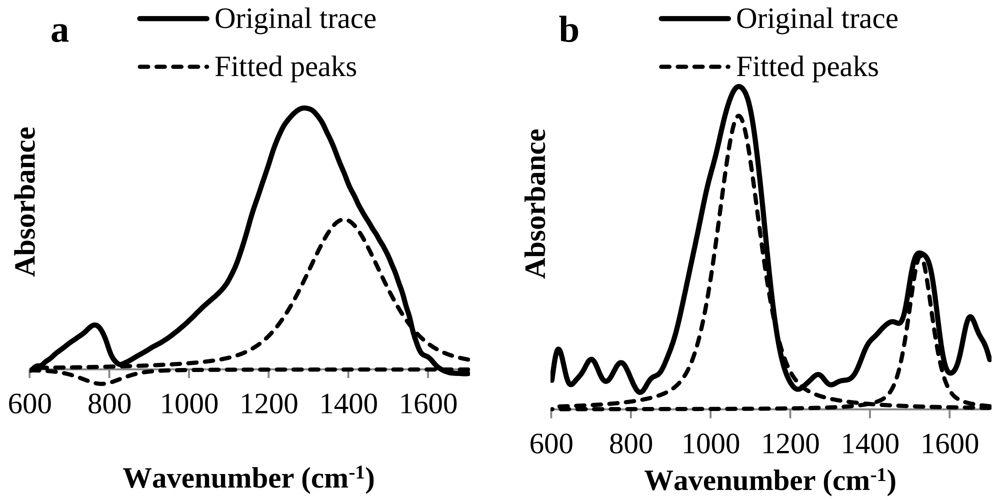

Fig. 9 Absorbance mode IR spectra of (a) h-BN thin film (b) c-BN thin film

We explored surface topography of coatings under SEM. The micrographs of BN coated and uncoated stainless steel surfaces are shown on Fig.9. On the micrograph of as-rec SS sample, we can easily detect the grain boundaries of virgin steel. In order to avoid any unfavorable effect on film growth from surface features like this, most of the steel samples were mirror-like polished attaining a uniform and almost flawless surface for film growth. Surface topography of as-rec and polished substrates after 3 h h-BN deposition, as well as luster-finished c-BN coated steel substrate are presented on Fig.9.

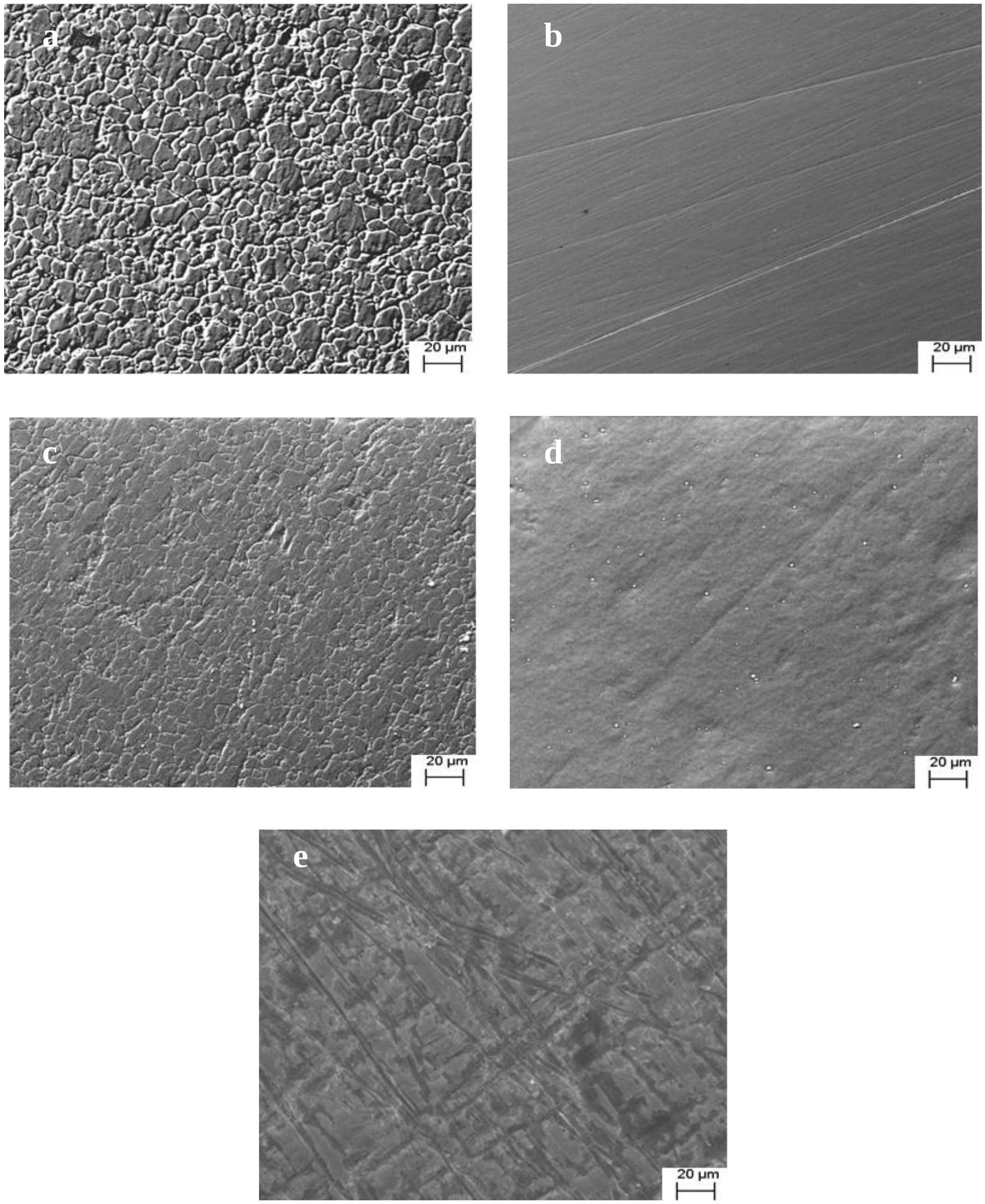

Fig. 10 SEM micrographs SEM images of (a) as-rec SS (b) polished SS (c) h-BN as-rec (d) h-BN polished (e) c-BN lustred

Arithmetic average surface roughness (R_a) values of each sample group were listed in Table 5. After h-BN deposition on polished surfaces, R_a values were measured around 7.93 nm. Additionally, R_a values of c-BN thin film coatings on luster-finished samples were obtained as 152.38 nm. According to SEM images and R_a values, we did not detect a significant change on the surface roughness of thin film coated surfaces compared to uncoated substrate upon the application of PVD [103]. Furthermore, since there is a significant discrepancy between two roughness values of h-BN and c-BN thin films which might consequently influence bacterial adhesion indirectly, we decided to deposit h-BN on as-received steel surfaces for control purposes. R_a values for as-received steel surfaces were determined around 102.83 nm which is a value that can relate to c-BN roughness.

Table 5 Surface roughness (Ra), contact angles with deionized water and diiodomethane and surface free energy of each group

	R_a (nm)	**Contact angle**		**γ_s^d (mN/m)**	**γ_s^h (mN/m)**	**γ_{sv} (mN/m)**
		Water	Diiodomethane			
As-rec SS	126.3	84	48	35.2	3.2	38.4
h-BN as-rec	102.8	57	45	37.1	15.4	52.5
Polished SS	5.3	95	60	28.8	1.3	30.1
h-BN polished	7.9	72	48	35.1	7.9	43.0
c-BN lustred	152.4	58	46	36.3	14.7	51.0

Fig.10 elucidates how *E. coli* colonies behave on uncoated and BN coated stainless steel substrates. According to cell culture experiments, we observed a remarkable antibacterial activity accompanying a decrease in *E. coli* amount around 88% on c-BN coatings compared to polished bare SS substrates. On the contrary, we observed an increase in *E. coli* amount about 71% on h-BN coated polished substrates relative to bare SS substrates. Meanwhile, we observed the same trend on h-BN coated as-received surfaces, where *E. coli* adhesion increased around 50%.

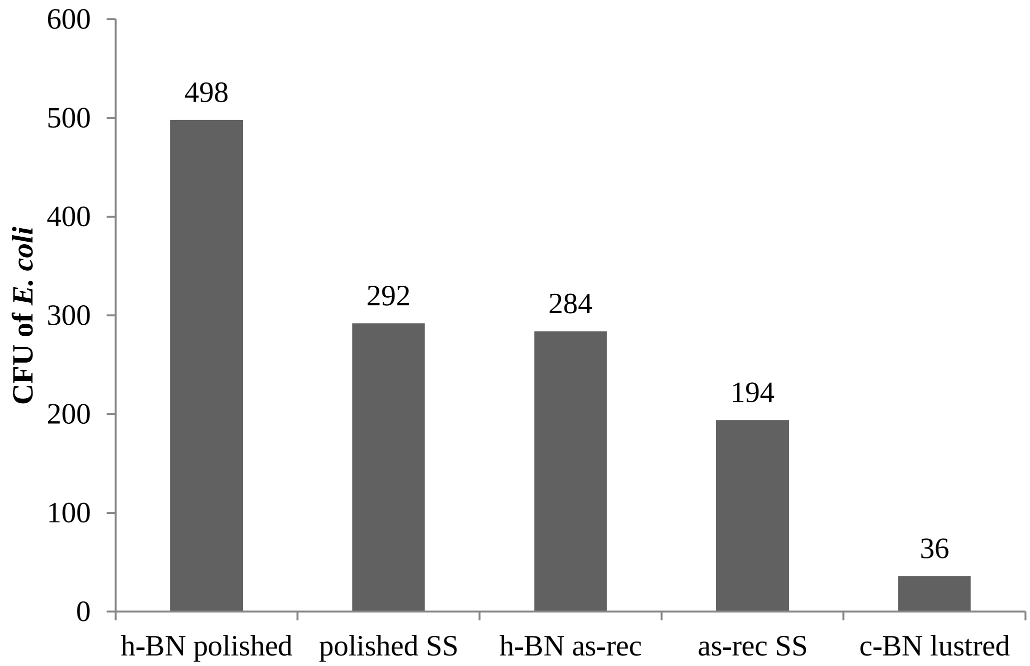

Fig. 11 The quantity of *E. coli* colonies after 4 h incubation

SEM micrographs recorded after bacterial cell culture tests also corroborated above data. *E. coli* colonies accumulated at certain regions of uncoated as-rec SS substrates could be readily seen in Fig.11a. Additionally, on polished bare SS surfaces, colonies randomly accommodated. However, when h-BN coatings were spatially explored under SEM, we witnessed a notable amount of increase of bacteria colonization all over the samples as shown in Fig.11c and Fig.11d. Though, c-BN coatings on steel surfaces allowed almost no *E. coli* adhesion as demonstrated in Fig.11e.

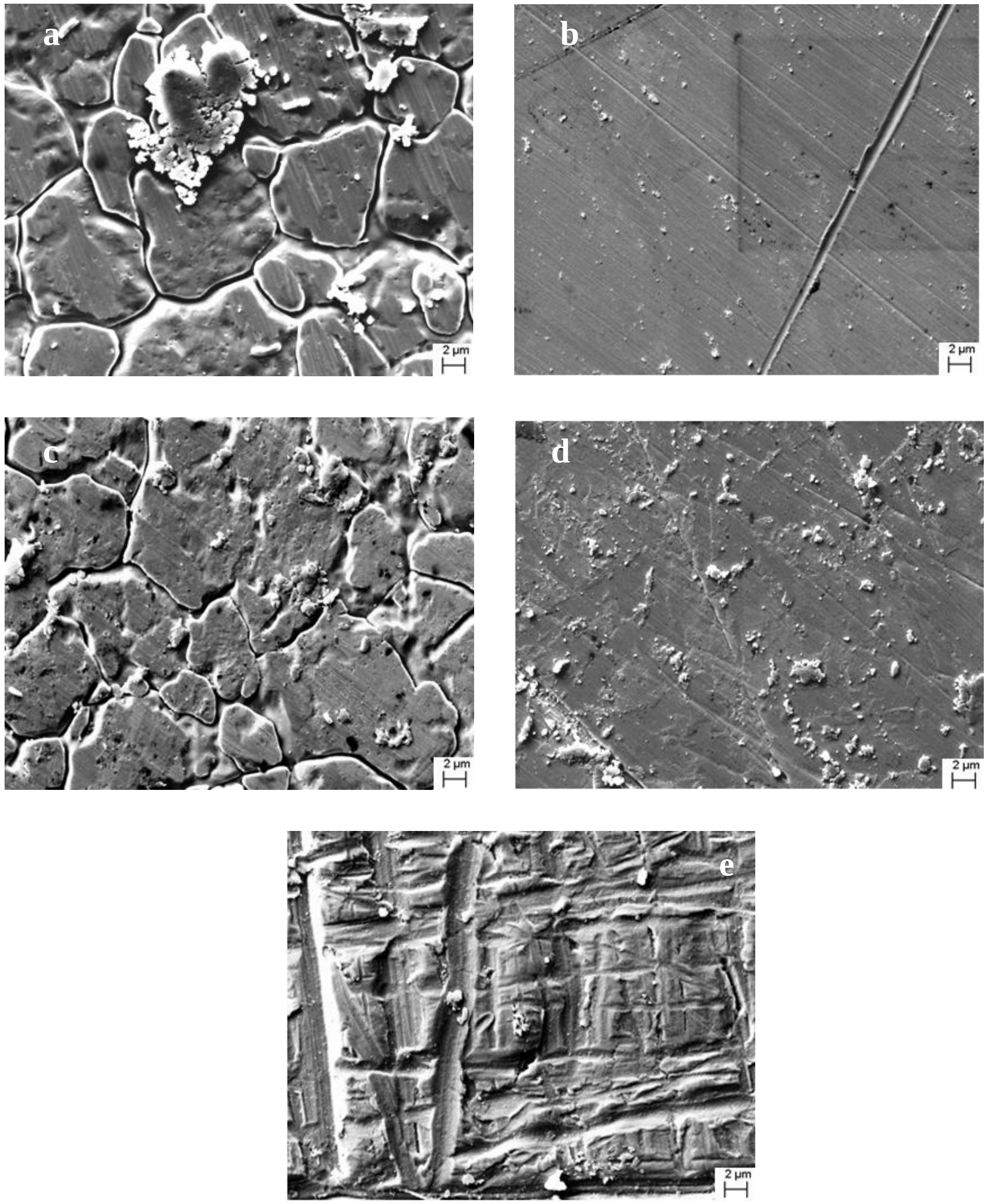

Fig. 12 SEM micrographs of (a) as-rec SS (b) polished SS (c) h-BN as-rec (d) h-BN polished (e) c-BN lustred after bacterial tests

Generally rough surfaces are recognized as favorable terrain for bacterial attachment owing to the fact that they provide larger contact area [42, 49, 51, 104].Yet, according to data collected during our experiments, we observed a contrasting phenomenon to this general fact. For example, even though c-BN coated substrate exhibited the highest R_a, the least bacterial adhesion was observed on it according to data given on Table 5 and Fig.9. Indeed, we recorded the highest bacterial accumulation on h-BN coated and uncoated polished SS samples which have the lowest surface roughness. Furthermore, h-BN thin films coated to polished SS has around 20% more bacterial adhesion relative to h-BN coated to as-rec SS which is in inverse proportion. Therefore, we could not establish a succinct correlation between surface roughness and bacterial adherence similar to numerous researches [45, 47, 48, 51]. More importantly, the length scale between the roughness asperities and the conditioning layer that is made up of organic and inorganic particles should be similar, since greater roughness might provide less contact area depending on the size of the adsorbing specie [105]. As a result, it is hard to make a conclusion about the effect of surface roughness on bacterial adhesion alone excluding other physico-chemical parameters of the surface as well as a comparable scale based on the size of the surface asperities and the adsorbing entities [45, 47].

In Table 5, we recorded contact angle measurements performed with both deionized water and diiodomethane. With respect to Owens-Wendt theory, we calculated dispersive force (non-polar) and hydrogen bonding (polar) components of surface free energy (SFE). Table 5 also tabulates total SFE of each group that is equal to sum of these two components. All untreated SS surfaces following h-BN and c-BN deposition become more hydrophilic. γsd of all uncoated and BN coated SS samples were around 36 mN/m with only exception of polished SS. The difference between as-received SS and polished SS probably proceed from different surface microstructure and roughness [106]. The incorporation of nitrogen and boron on SS surfaces increased the total SFE in consequence of a rise in γsh component due to the strong polarity between boron-nitrogen bonds [107, 108]. However, we observed opposite trends on bacterial accumulation, even if both h-BN and c-BN deposition enhanced polarity, hence total SFE. Many researches driven by other groups also found no correlation between SFE and bacterial adhesion because other experimental factors and surface parameters, such as surface morphology, surface chemistry, suspension medium, type of bacteria, and temperature might contribute to cumulative effect on bacterial adhesion [38, 47, 55, 106, 109].

Fig.12 demonstrates the force vs. distance curves of h-BN and c-BN coated samples in BHI medium. Experiments were performed with a silicon nitride tip connected to a microfabricated cantilever. During AFM force measurements, the force determined from the deflection of a cantilever is measured as a function of sample displacement [110, 111]. The direct measurements of surface forces could be helpful to discern the surface charge of the materials; however, it is important to recognize which forces are acting between the surface and the AFM tip [112, 113]. Generally, electrostatic forces play an active role in aqueous medium [112]. In contact mode, we should consider the repulsive force as essential for the cantilever and the sample to detach from each other [110]. According to the interaction between negatively charged silicon nitride tip and BN coated surfaces, the force-displacement curves showed that h-BN coated surfaces was more negatively charged in BHI broth than c-BN with an amount around 25 nN.

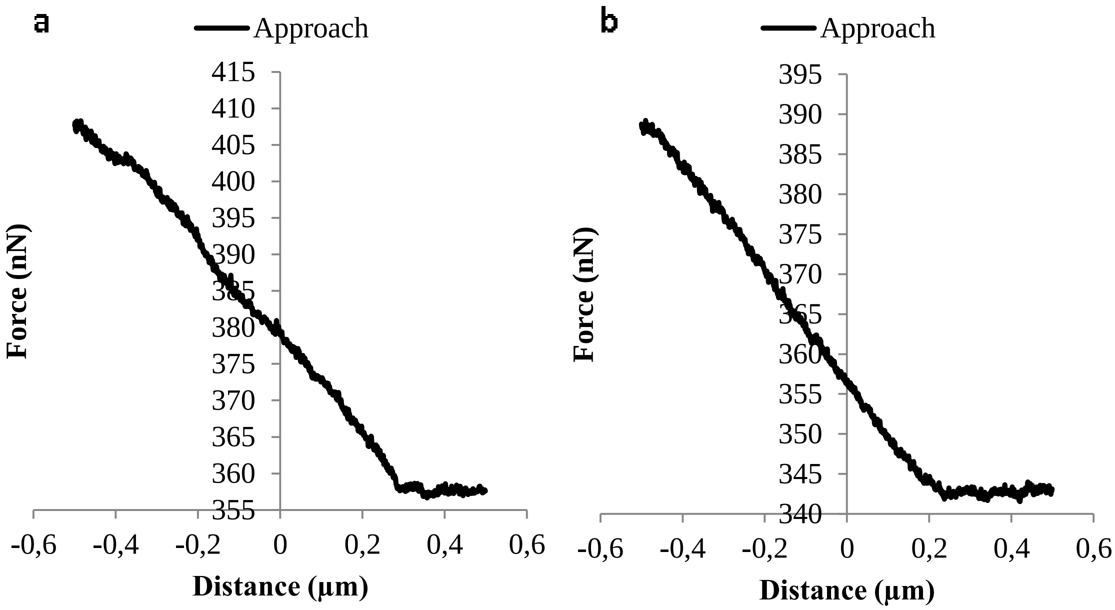

Fig. 13 Force-distance curves in BHI (a) h-BN polished (b) c-BN lustred

Fig.13 demonstrates dynamic mode AFM images of h-BN and c-BN coated substrates in BHI broth. There is an obvious interaction between h-BN surface and ingredients of BHI, since we can notice good quantity accumulated on its surface, whereas no deposition occurred on c-BN surface. The difference between the behaviors of two surfaces may play a determinant role on bacterial adhesion mechanism. Most of the solid bodies as well as microorganisms immersed in an aqueous medium at neutral pH bear a negative surface charge [58, 62, 63, 114]. When the surface placed in aqueous liquid charged, it results in redistribution of ions in solution. Then, surface starts to attract the ions of opposite sign, while repel them of same charge [114]. By this way, more negatively charged h-BN surface may attract positively charged ions in the broth, such as Na+ which may allow closer contact between the bacteria and substrate surface and enhance bacterial adsorption [115, 116]. Bacteria can directly adsorb on a solid surface through the cell wall [117] that has a great propensity for specific cations such as

Na+, Ca2+ and Mg2+. These ions are directly linked to the wall matrix and induce bacterial accumulation [111, 117-121]. Adsorption of cations onto a negatively charged surface may be much quicker than cell migration in a liquid medium. Hence, negatively charged bacterial cell surface can attach on a negatively charged substratum surface via cation bridging mechanism [117].

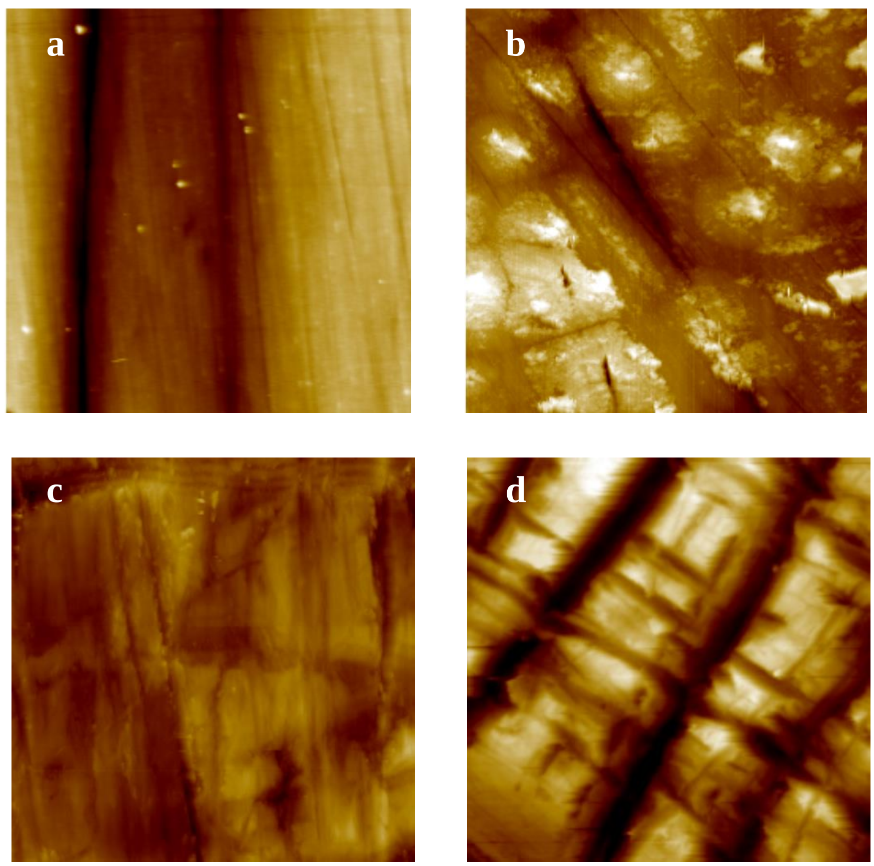

Fig. 14 Dynamic mode AFM images of h-BN polished in (a) air (b) BHI (c) c-BN lustred in (a) air (b) BHI

2.4 Conclusion

In this study, we examined the antibacterial effect of different crystallographic structures of BN thin films when coated on 316L grade steel. In summary, we attested that c-BN coated SS samples demonstrated a remarkable decrease in the number of E. coli while h-BN coated surfaces favors bacterial adhesion. We relate this reduction and rise in bacterial accumulation to the difference in spatial arrangement of BN atoms in space and thereof to surface charge. Similar to carbon, BN forms two equilibrium phases: one is sp2 hybridized hexagonal structure and the other is sp3 hybridized cubic structure. Due to its layered structure, we suspect that top layer of h-BN has some ionic character because of significant electronegativity difference between two dissimilar atomic species unlike carbon in graphite where carbon is the only element forming it [108, 122]. Indeed, we determine more negative charge on h-BN compared to c-BN coatings via zeta potential and AFM force-distance measurements. In conclusion, we suspect that subtle electrostatic forces on the top layer of h-BN coatings might orchestrate the microorganism attachment onto this surface while c-BN with pretty much balanced sp3 structure do not induce any columbic forces to facilitate bacterial adhesion.

CHAPTER 3

3. INVESTIGATION OF CATIONIC PEPTIDE COATED SILICONE RUBBER SURFACES FOR ANTIMICROBIAL PURPOSES

3.1 Introduction

In recent years, the use of indwelling medical devices, such as catheters, contact lenses, heart valves, prosthetic joints, pace makers and voice prostheses has considerably expanded to achieve a better life quality and increase patient survival rate [36, 40, 123]. Nevertheless, these biomaterials often generate inevitable hospital-acquired infections within implantation, especially when they are used for extended periods. The initiation of a persistent infection is commonly associated with colonization of surfaces by microorganisms in the form of biofilms [124-126]. Biofilms are generally differentiated from sporadic attachment of microorganisms with their dense population of microbial cells encased in an extracellular polysaccharide matrix which facilitates adhesion and structural integrity of the cells [36, 40, 127-130]. Compared to planktonic (free-floating) organisms, biofilm-associated cells exhibit extremely high resistance to antimicrobial agents [4, 36, 131, 132].

Catheters, particularly intravascular (IVC) and urinary (UC) catheters, are especially essential in the successful management of many patients' lives with a critical or chronic disease [133, 134]. The specific advantages derived from catheter applications, however, often are balanced with life-threatening microbial contamination on their external surface or inner lumen [40, 133, 134]. IVC-related infections are mainly blood stream infections, septic thrombophlebitis, endocarditis and other metastatic infections [135] that are frequently associated with the presence of coagulase negative *Staphylococci, S. aureus, S. epidermidis, C. albicans P.aeruginosa, K. pneumonia* and *Enterococcus faecalis* [40, 133-140]. Besides, over 40% of nosocomial infections are those of urinary tract, among which 80% found mostly in catheterized patients [141-145]. In 2012, Djeribi et al. reported that 25% of patients undergoing short-term urinary catheterization with less than 7 days acquired infections. Indeed the risk of developing an infection increases around 5% daily with longer catheterization [146]. For all long-term (more than 28 days) catheterized patients, the estimated risk of infections is 100% [146, 147]. The most commonly isolated microorganisms from UC were listed as *S. epidermidis, Enterococcus faecalis, E. coli, Proteus mirabilis, P. aeruginosa, K. pneumonia* and *Candida spp.* [40, 124, 126, 143, 146].

The wide diversity of causative organisms in biofilm infection has motivated the development of materials with broad-spectrum antimicrobial activity [126]. In spite of several strategies developed for the control of biofilm deposition on catheters, including antibiotics [148-150], quaternary ammonium compounds [151-154], phenol derivatives [155], titanium oxides [156], silver coatings/impregnation [142, 157], hydrogel-coatings [158] and cationic surfactants [159], their use is often restricted by their potential toxicity and inefficiency [5, 36, 131, 139, 142, 160, 161]. In 2000, Van de Belt et al. stated that antibiotic-releasing agents lead to the emergence of antibiotic resistant microbial species [162]. Moreover, some currently accessible antifungal compounds such as, polyene and azole antimycotics and DNA analogues holds toxic as well as unfavorable side effects [163].

Because of the increase in microbial resistance to conventional antibiotics, most of the researches in this area are driven by the urgency to develop novel antimicrobial agents [32, 164-168]. Antimicrobial peptides (AMP), the natural antibiotics already existing in the defense mechanisms of all species of life [35], have a broad spectrum of antimicrobial activity to combat bacteria, fungi, protozoa, and viruses [33, 34, 131, 164, 166, 169-171]. Because of Lys and Arg residues in their main chain AMPs are highly cationic and typically short in length (10-25 amino acids) with molecular weights (M_w) between 1 and 5 kDa. They have an amphipathic character in which a hydrophobic region that interacts with lipids and a hydrophilic region attracting water or negatively charged surfaces do exist together [32, 34, 35, 171]. Cationic peptides generally do not cause any bacterial resistance. They induce a high affinity to negatively charged microbial surfaces and membranes, however, do not exhibit a tendency to attack mammalian cells which have no net charge [32, 131, 164, 171-173]. Therefore, there are few promising attempts employed to design antimicrobial coatings using these natural substances on surfaces via physical adsorption or covalent immobilization [36, 52, 131, 174].

Haynie et al. in their work published in 1995, observed that some AMPs, such as magainin, cecropin and defensin when covalently grafted onto an ethylene-diamine functionalized polyamide resin exhibited lethal activity against *E.coli*, *S. aureus*, *B. substilis* and *K. pneumonie* as well as *C. albicans*. More importantly, when they examined the suspension where functionalized polyamide resin kept, they recorded no dissolved or hydrolyzed peptide in it. This indicates retention of the antimicrobial activity for prolonged periods on modified surfaces as a result of covalent immobilization [174]. Willcox et al. tested a synthetic peptide melimine both physically adsorbed and chemically conjugated onto commercial contact lenses. Physically adsorbed peptide surfaces demonstrated almost 80% decrease in both *P. aeruginosa* and *S. aureus* amount on melimine adsorbed lenses. Furthermore, chemically attached peptide surfaces exhibited more than 70% reduction in viable bacteria [36]. The research driven by Humblot et al. showed antibacterial performance of covalently bound Magainin I on the self-assembled monolayer (SAM) of mixed 11-mercaptoundecanoic acid and 6-mercaptohexanol (ratio 1:3) on gold surfaces. They not only revealed more than 50% reduction in bacterial adhesion, but also reported no peptide release into the bacterial suspension [131]. In addition, De Prijck and co-workers covalently grafted two synthetic versions (Dhvar 4 and Dhvar 5) of the salivary peptide histatin to PDMS surfaces. According to their results, Dhvar 4 functionalized PDMS yielded the highest disruption to *C. albicans* biofilm with %90 reduction [52].

Bovine lactoferrin which is 80 kDa iron-binding glycoprotein secreted in mammalian milk, tear, saliva and urine is another protein that exerts a wide range of antibacterial, antifungal and antiviral performance. However, a peptide fragment derived from N-terminal region of lactoferrin has more potent lethal activity towards pathogens [166, 175-181]. This region is commonly called cationic peptide Lactoferricin B (LFB) and is dissected from lactoferrin by pepsin enzyme via proteolytic cleavage [166, 175, 179-184]. LFB generally made up of 25 amino acid residues with the sequence of FKCRRWQWRMKKLGAPSITCVRRAF [166, 176, 177, 181], represented in Fig.14. It also contains a single disulfide bond between residues Cys19 and Cys36 and forms a β-sheet structure [166, 180]. The sequence involves several hydrophobic and positively charged residues, which can interact with bacterial cell membranes to alter their permeability [166, 179, 180].

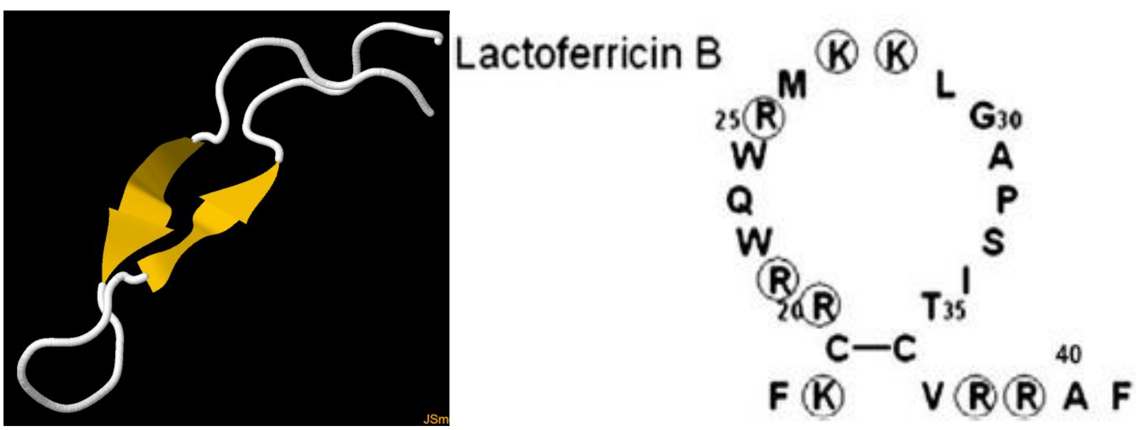

Fig. 15 The structure of LFB and its amino acid sequence [185, 186]

Polydimetylsiloxanes (PDMS) is a moldable silicon-based rubber consisting of repeating units of $– OSi(CH_3)_2O –$, shown in Fig.15 [187-190]. Among other polymeric systems, PDMS possesses various advantages, including its elastomeric nature, biocompatibility, non-toxicity, gas permeability, excellent optical transparency, relative chemical inertness, ease of molding, and low manufacturing costs [187, 189-194]. Although the favorable and profitable properties of PDMS make it an ideal candidate for numerous health-care applications- in orthopedics, catheters, drains and shunts [187], the major drawbacks of pure PDMS are its low surface free energy (hydrophobicity) and extremely low surface reactivity that often render the possible PDMS applications [189, 190, 193, 194]. Hence, there are a number of physical and chemical surface modification methods developed by introducing reactive functional groups onto the polymer surface [188-190, 193-195]. Oxygen plasma, UV/ozone treatment and corona discharge are most commonly used physical modification techniques to create more hydrophilic PDMS surfaces [189, 190, 193-195]. However, neither of these techniques can ensure to hold oxide groups permanently on PDMS surfaces since PDMS rubber regains its hydrophobicity sometimes in less than couple of hours after exposure to air [189, 193, 194, 196]. This phenomenon is known as hydrophobic recovery which mainly occur by migration of uncured PDMS oligomers from the bulk to the surface or the rearrangements of highly mobile polymer chains on the surface by flipping Si-OH bonds towards the bulk [189, 193, 194, 197-199].

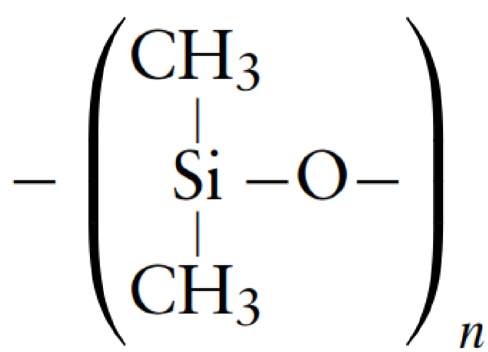

Fig. 16 The chemical structure of PDMS [187]

In the context of this research, we aimed to develop a novel anti-biofouling surface for silicone catheters based on lactoferricin B (LFB). With this intention we conjugated this cationic peptide onto biomedical grade PDMS surfaces. During experiments, ATR-FTIR was used to examine pristine PDMS surfaces as well as to validate the surface modification via characteristic frequencies of surface modifying agent LFB. Furthermore, water contact angle data were measured to explore change in the hydrophilic/hydrophobic behavior of the sample surfaces. Surface topography and features of substrates were observed under confocal microscopy and scanning electron microscopy (SEM). Bacterial tests were performed with two of the most frequently isolated hospital pathogens from intravascular and urinary catheters, *S. epidermidis* and *P. aeruginosa*. SEM was also utilized to demonstrate bacterial colonies attached on PDMS surfaces after 4 h incubation.

3.2 Experimental

3.2.1 Materials

Polydimethylsiloxane (PDMS) Elastosil® R plus 4305/60 was supplied by Wacker Chemie AG (München, Germany). Lactoferricin B (LFB) was provided by GL Biochem (Shanghai) Ltd with more than 98% purity. The amino acid sequence of peptide was given as Phe-Lys-Cys-Arg-Arg-Trp-Gln-Trp-Arg-Trp-Lys-Lys-Leu-Gly-Ala-Pro-Ser-Ile-Thr-Cys-Val-Arg-Arg-Ala-Phe with 3180.86 kDa of molecular weight. Carboxyethylsilanetriol (CEST) disodium salt, %25 in water was purchased from Gelest, Inc. (Morrisville, PA). 2-(*N*-morpholino) ethanesulfonic acid (MES) buffer was purchased from Pierce Protein Biology Products (Thermo Fisher Scientific Inc., Rockford, IL). Undecylenic acid (UDA) and brain heart infusion (BHI) was provided from Merck (Germany). 1-Ethyl-3-(3-dimethylaminopropyl) carbodiimide (EDC), *N*-Hydroxysuccinimide (NHS), phosphate buffered saline (PBS), FT-IR grade potassium bromide (KBr) and all other organic solvents were purchased from Sigma-Aldrich (Germany).

3.2.2 PDMS extraction

To attain hydrophilic PDMS surfaces with long-term stability after oxygen plasma treatment, samples were subject to series of solvents to discard low molecular weight uncured oligomers from the bulk phase as described by Vickers et al. First, pieces of PDMS were soaked in 200 ml of triethylamine solution at room temperature for 2 h with stirring. After 1 h, triethylamine solution was replaced with fresh one. Then, substrates were placed in 200 ml of ethyl acetate at room temperature and mixed for 2 h. The liquid was refreshed after 1 h. The final solvent was acetone in which PDMS were immersed for 2 h at 25 °C with stirring. Finally, pieces were kept in an oven at 65 °C for 3 h to be completely dried [200].

3.2.3 Surface activation by oxygen plasma

Plasma generates high energy species, such as electrons, ions and radicals which are independent of an atom or molecule [193, 195]. Plasma treatment can be performed under gases, including oxygen, nitrogen and hydrogen which are ionized so as to react with the material surface to create new chemical functional groups [194]. Oxygen plasma interacts with the siloxane backbone of PDMS to create Si-OH groups and SiO_x silica-like layer with richer oxygen content than the bulk PDMS [193, 195].

PDMS surfaces were activated in Femto Science Cute-B (Korea) low-pressure plasma system equipped with a RF power supply of 13.56MHz frequency. Oxygen gas with 99.5% purity was introduced into the vacuum chamber with a 70 x 100 cc/min gas flow rate. The power of the system was adjusted to 100 W and plasma excitation was conducted for 5 min to both sides of PDMS.

3.2.4 Surface modification by undecylenic acid (UDA)

Prior to the peptide conjugation on PDMS substrates, samples were modified by undecylenic acid (UDA) to create carboxylic acid groups on surfaces. The as-received PDMS was first rinsed with deionized water, then soaked in ultrasonic bath filling with 99.8% ethanol and dried under fume hood. After oxidation of PDMS surfaces by plasma treatment, samples were immersed in glass containers with enough UDA solution (1.2 g in a solution of 10 ml deionized water and 10 ml 99.8% ethanol) to generate a thin film on all PDMS sides. UDA solution containing glass bottles were kept in an oven at 80 °C overnight [190]. After that, UDA-modified PDMS were cleaned by ultrasonication for 10 min in deionized water, for 30 min in 50% ethanol (the solution was replaced with refresh one after 15 min) and in deionized water for another 10 min. At the end, samples were rinsed with deionized water and dried under fume hood.

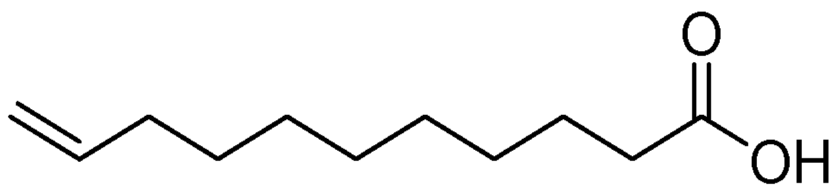

Fig. 17 The chemical structure of UDA [201]

3.2.5 Surface modification by carboxyethylsilanetriol (CEST)

In a different way to functionalize surfaces with carboxylate groups, a silane coupling agent CEST was used. This silanization reagent can quickly react with –OH groups of inorganic substrates without prior hydrolysis of alkoxy groups [202]. 1.8 ml of CEST (600 μl of CEST per 10 ml of buffer) was added into a beaker containing 30 ml of PBS (10 mM, pH 7.4). Then, O_2 plasma-treated PDMS pieces were placed into solution at room temperature and kept overnight for the reaction with continuous mixing. Following silanization, samples were washed with PBS several times. A final rinsing was done with 10 mM MES (pH 5.5) to prepare the surfaces for subsequent conjugation with amine-containing molecules [202, 203].

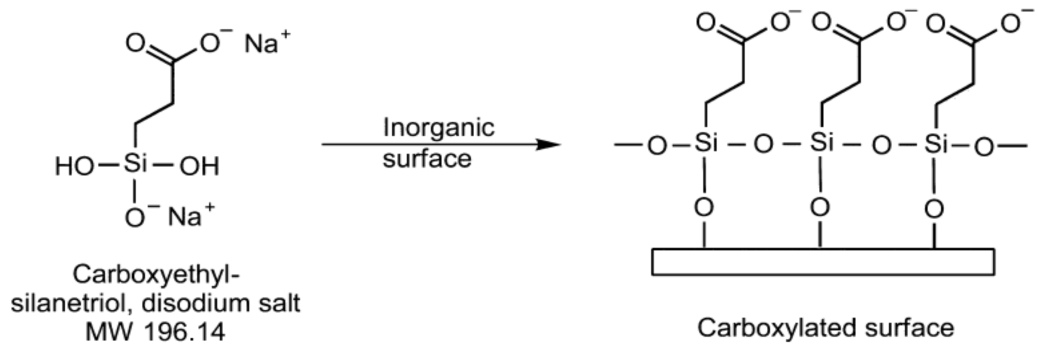

Fig. 18 Modification of carboxylate groups on an inorganic substrate by CEST [202]

3.2.6 Peptide conjugation

After generation of carboxylic acid groups on surfaces, UDA-modified PDMS pieces were immersed in 30 ml of phosphate buffer (0.1 M, pH 6.0) while CEST-modified PDMS strips were put into 30 ml of deionized water. pH of the water was adjusted to physiological pH, 7.4 by gradual addition of 0.1 M HCl or 0.1 M NaOH when necessary. Later, 36.7 mg of EDC was added with stirring to activate carboxylate groups on PDMS surfaces. Carbodiimides, mediate an amide linkage between carboxylate and amine groups without any auxiliary chemical structure between conjugating molecules, that is the reason they are also called zero-length cross-linking agents [204]. After 10 min, 6 mg of LFB was added together with 4.2 mg of NHS which provides stability to labile amide linkages [204]. The amounts of EDC and NHS were determined with respect to the concentration of LFB, and used 100 and 10 times excess of LFB for EDC and NHS, respectively. The reaction was allowed to continue for 2 h at room temperature. Finally, samples were removed from the mixtures and rinsed many times with deinozed water to get rid of unreacted peptides from the surface.

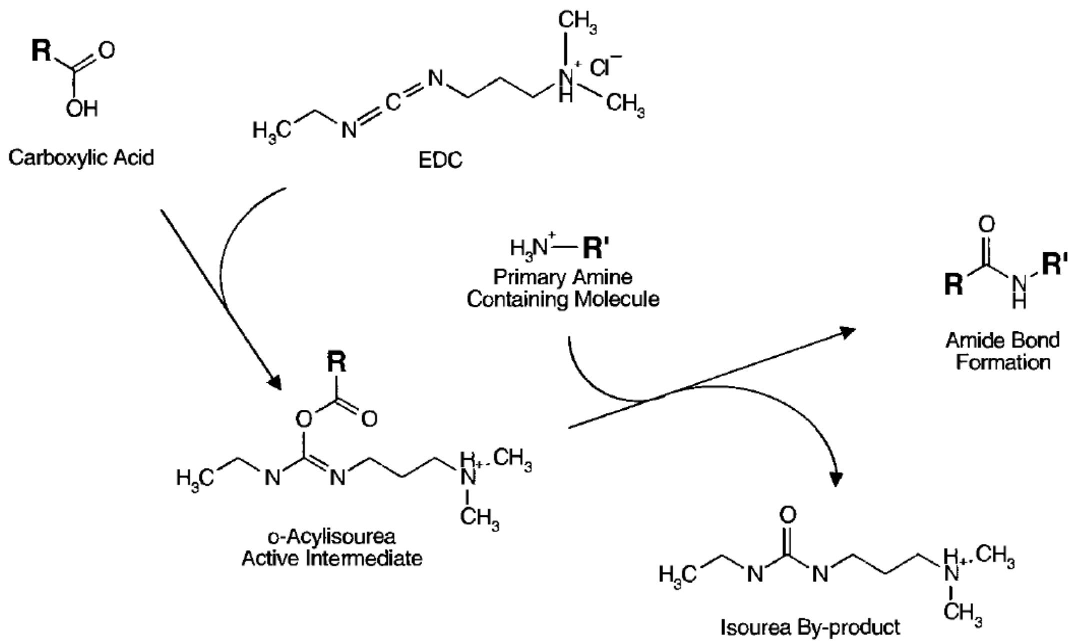

Fig. 19 Zero-length cross-linking by carbodiimide chemistry [204]

3.2.7 FTIR measurements

Each surface modification step was checked by ATR-FTIR (Bruker IFS55, Germany) in absorbance mode. The data was collected from 400 to 4000 cm^{-1} with a spectral resolution of 8 cm^{-1} and 32 scans. All measurements were performed at room temperature and atmospheric pressure. Only, the spectrum of Lactoferricin B was characterized in FTIR, thus samples are prepared with KBr salt as pellets. First, a little amount of LFB was placed into an agar mortar to be mixed with KBr salt. Then, the mixture was homogenously grinded to a smooth powder. 13 mm diameter pellets were prepared under the pressure of 5 tones for about 3 min. All spectra recorded were baseline corrected and smoothed via spectroscopy software (Grams Suite 9.1, Thermo Fischer Scientific, PA).

3.2.8 Water contact angle (WCA) determinations

Pure and modified PDMS surfaces were characterized by static sessile drop contact angle measurements (Attension Theta Lite Optical Tensiometer, Finland) to assess the change in surface hydrophilicity with respect to modification. A 2.00 μl of deionized water droplet was placed on the sample surface by a syringe pump at room temperature. Each measurement was recorded for 3 s in which 36 images were captured and mean contact angles were determined from at least six different positions on the specimen.

3.2.9 Confocal microscopy

Compared to conventional optical microscopy, confocal microscopy builds sharper and better-resolved images as well as three-dimensional (3D) reconstruction of specimen volume by collecting serial thin sections recorded along the vertical axis. It is also able to control the depth of field and reject the background information to prevent image degradation. The image can be recorded by reflection of light over the substrate or excitation of fluorescence which eventually emits from dyes applied to the sample [205-207].

The working principle of confocal microscopy was schematically represented in Fig.19. The laser excitation source emits the light which goes through a pinhole aperture. Then, the light is reflected by a dichromatic mirror and scanned across the substrate in a defined focal plane. After that, it passes back through the mirror and focused as a confocal point at the detector pinhole aperture. As seen in figure, out-of-focus light rays are not detected by the photomultiplier and not presented in the final image [205-207].

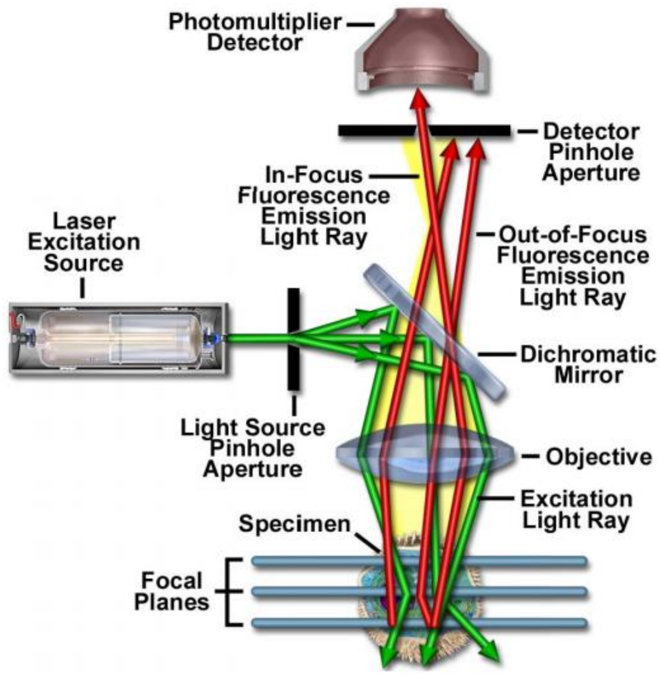

Fig. 20 Schematic diagram of confocal microscopy [205]

We operated a Leica, TCS SP5 laser scanning confocal microscope in RT 30/70 (30% reflection 70% transmission) with an Argon laser illuminating at wavelengths of 488-517 nm. Imaging was achieved with %10 power with a resolution of 8 bits and scan speed of 400 Hz.

3.2.10 Scanning electron microscopy (SEM)

SEM was used to explore surface topography of the samples and how bacterial colonies acted on different surfaces during 4 h incubation period. Prior to electron microscopy, all substrates were gold coated by sputtering method. This process was carried out in order to render samples conductive so as to avoid charging and avoid any beam damage on the polymer samples thereof. SEM micrographs were captured at 2000x-5000x magnifications with an operating voltage of 10 keV.

3.2.11 Bacterial culture

The coagulase-negative *Staphylococcus epidermidis,* a gram-positive skin and mucous membrane microflora bacterium, is mainly associated with infections encountered due to indwelling medical devices, especially intravascular catheters, prosthetic joints and artificial heart valves. Infections caused by *S. epidermidis* generally end up with diseases like endocarditis, pneumonia, acute sepsis and sometimes with the loss of the patient [136, 208, 209].

Pseudomonas aeruginosa is an aerobic gram-negative bacterium, one of the mostly encountered opportunistic nosocomial human pathogens. It is particularly responsible for pneumonia, hospital-acquired urinary tract infections and bloodstream infections [210-212].

Samples were tested by *S. epidermidis* ATCC 12224 and *P. aeruginosa* ATCC N145 provided from the collection of Medical Microbiology Department of Ankara University, School of Medicine. First, bacteria were cultured in brain heart infusion (BHI) broth, and then streaked on blood agar plates and grown overnight at 37° C. Later, microorganisms were harvested by centrifugation at 300 rpm for 10 min and washed three times with PBS. Right after, strains were resuspended in BHI. A droplet of diluted bacterial suspension was placed on Neubauer glass so as to calculate the concentration of bacteria that was adjusted to about 10^6 CFU/ml [97].

3.1.1 Bacterial adhesion tests

Bacterial tests in static soaking method were employed after 4 h incubation. Each sample was immersed in 4 ml of bacterial suspension and then incubated at 37 °C for 4 h periods. Following incubation, substrates were rinsed three times with PBS to remove any nonattached bacteria and then placed in 4 ml of PBS buffer solution. Subsequently, they were vortexed for 30 s to detach bacteria from the sample surfaces. 10 µl of liquid was inoculated on agar plates and allowed to grow at 37 °C overnight. Finally, colony forming units (CFU) on each agar plate was counted to determine antibacterial performance of the specimens according to the formula below [97]:

$$A\,(\%) = \frac{[\text{mean CFU (Pristine PDMS)} - \text{mean CFU (LFB coated PDMS)}]}{\text{mean CFU (Pristine PDMS)}} \text{x}100$$

3.3 Results and Discussion

In this study, in order to render PDMS with anti-biofouling properties, we physically adsorbed or covalently attached LFB to PDMS surfaces. ATR-FTIR characterization is a very competent technique to comprehend the substrate surfaces before and after the surface modifications. Hence, we employed FTIR spectroscopy at every stage of the surface alterations either done via physical or chemical means. Fig.20 presents the IR spectrum of LFB with its characteristic peaks, as listed in Table 6. NH stretching from amide groups exhibits an intense band around 3300 cm^{-1} and a weaker band near 3100 cm^{-1}. Moreover, it shows another strong peak at 1680-1630 cm^{-1} due to the carbonyl (C=O) stretching vibrations. The CNH vibration involving both NH bending and C-N stretching absorbs IR light strongly close to 1550 cm^{-1} [213-215]. Thus, these three strong bands were tracked after peptide conjugation on PDMS surfaces.

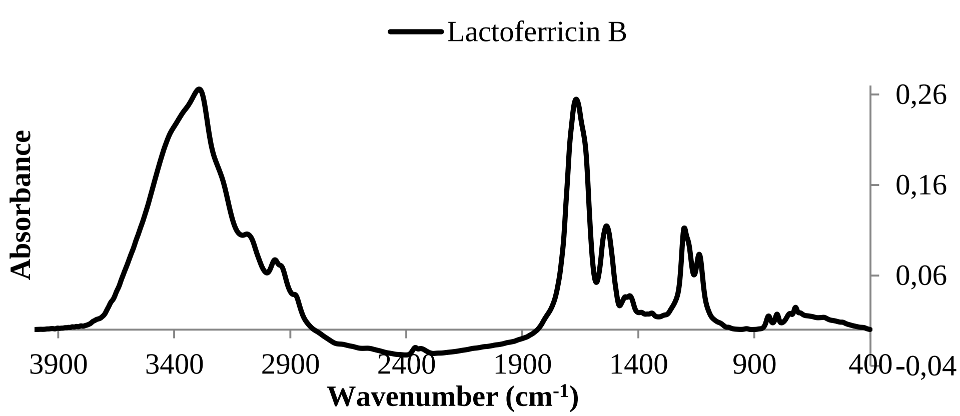

Fig. 21 The IR spectrum of LFB

Table 6 Characteristic peaks of LFB and their assignments [213-215]

Wavenumber (cm^{-1})	**Assignments**
3293	Amide A (NH stretching)
1668	Amide I (Carbonyl (C=O) stretching vibration)
1537	Amide II (CNH vibration)
1455	$\delta(CH_3)$, Leu, Val, Ala
1437	$\delta(CH_2)$, Lys, [Glu, Arg]
1202	CNH
1137	NH_2 bending

Key: Leu – leucine; Val – valine; Ala – alanine; Lys – lysine; Glu – glutamic acid; Arg – arginine

The IR spectra of pristine and O_2 plasma treated PDMS were demonstrated in Fig.21. In this figure, PDMS surface after O_2 plasma treatment exhibits a broad absorption band around 3450 cm^{-1} which could be associated with O-H stretching of water molecules adsorbed on silanol interface as a thin layer [216]. The characteristic peaks given in Fig.22 and Fig.23, validates the peptide conjugation following UDA and CEST modifications, respectively. Fig.22a indicates the IR spectra of PDMS modified by undecylenic acid which additionally presents a peak at 1713 cm^{-1}, corresponding to C=O stretching. This evidence is a strong confirmation of the surface alteration [190, 216]. Moreover, we could not detect any trace of C=O bond in the IR spectrum of CEST-modified PDMS, as shown in Fig.23a. Table 7 shows the spectral values of each sample before and after surface modification with peak assignments.

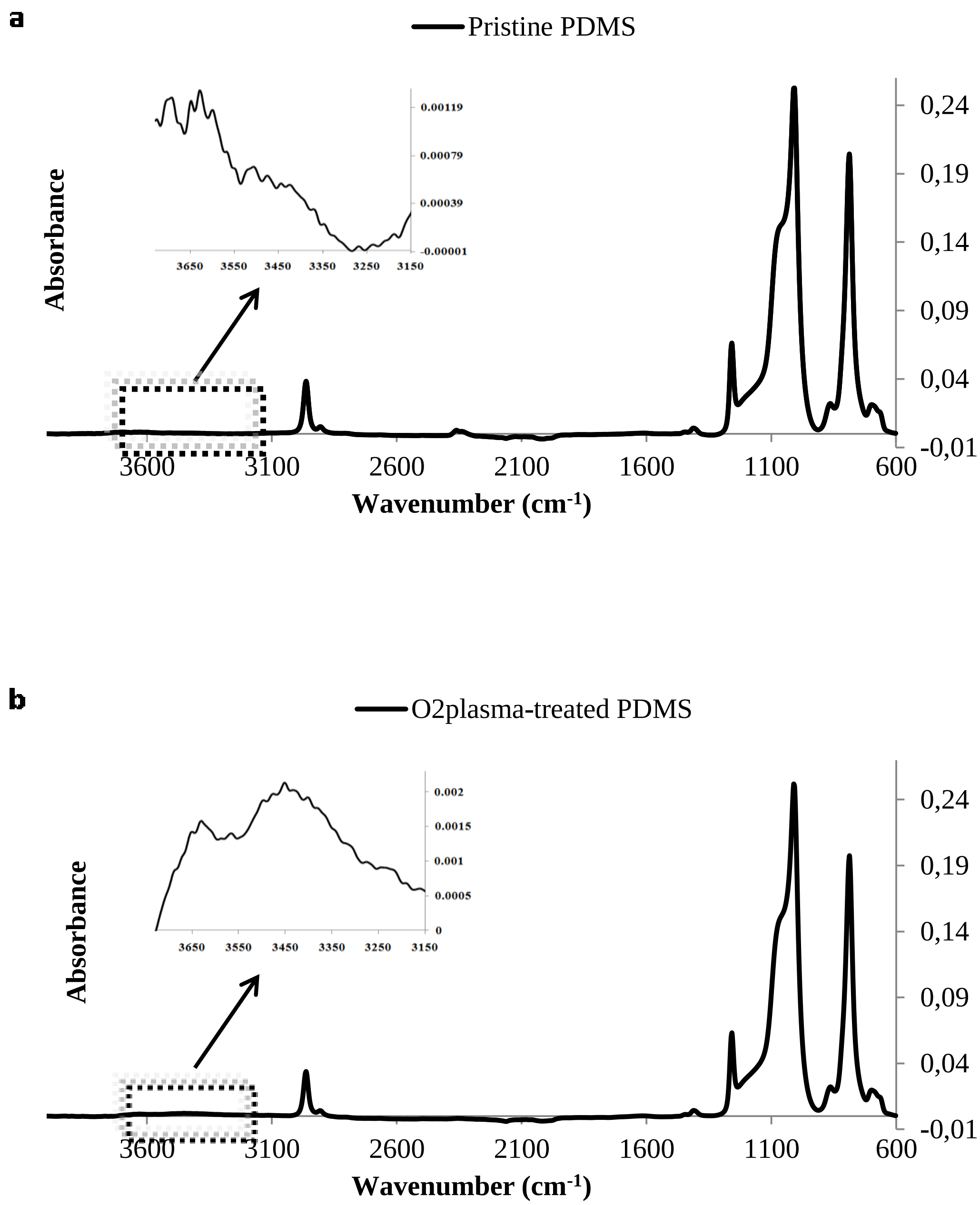

Fig. 22 The IR spectrum of (a) pristine PDMS (b) O_2 plasma-treated PDMS

Table 7 PDMS surfaces before and after modifications with peak assignments [213, 215-217]

Assignments	**Pristine PDMS**	**Extracted PDMS**	**O_2 plasma-treated PDMS**	**UDA-modified PDMS**	**CEST-modified PDMS**
O-H stretching	-	-	3450	-	-
Methyl CH	2963	2964	2963	2963	2963
C=O	-	-	-	1713	-
CH_3 asymmetric deformation	1411	1410	1410	1411	1411
CH_3 symmetric deformation	1258	1258	1256	1258	1258
Si-O-Si asymmetric stretching	1009	1009	1009	1009	1009
Si-C stretching	863	864	863	863	863
Si-$(CH_3)_2$	788	788	788	788	788
Surface	697	697	698	697	697

After LFB immobilization on carboxylated PDMS surfaces, ATR-FTIR measurements demonstrated the characteristic peptide frequencies (Fig.22b and Fig.23b) belonging to LFB. This evidence corroborates the successful conjugation of the cationic peptide on PDMS substrates. Intense Amide I and Amide II bands at 1637 cm^{-1} and 1538 cm^{-1} respectively, is a strong confirmation of UDA-modified LFB coated PDMS surfaces. CEST-modified LFB coated PDMS surfaces also represented Amide I frequency at 1649 cm^{-1} and Amide II frequency at 1552 cm^{-1}, however, the intensities of these peaks are much more weaker compared to UDA-modified PDMS.

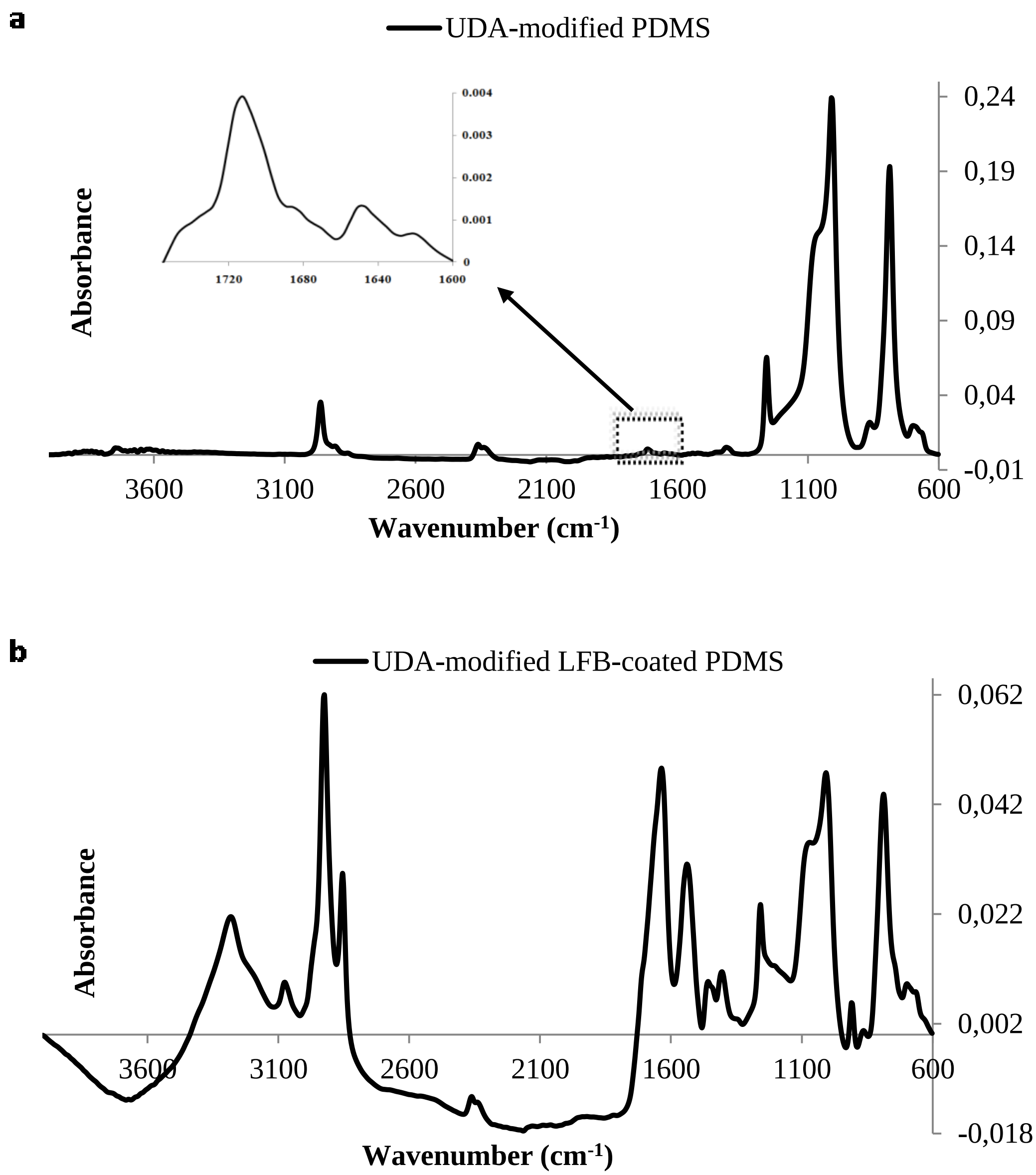

Fig. 23 The IR spectrum of (a) UDA-modified (b) UDA-modified LFB-coated PDMS

a

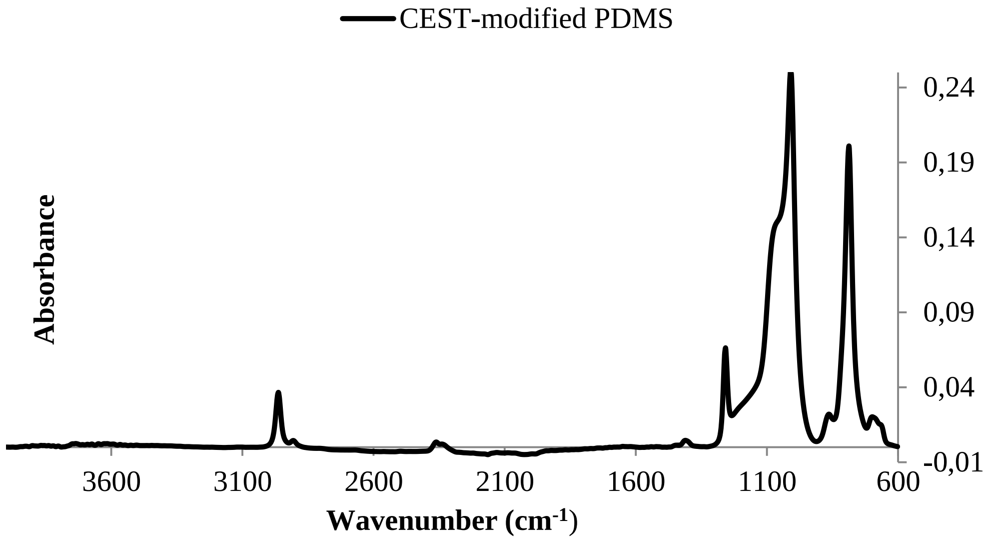

b

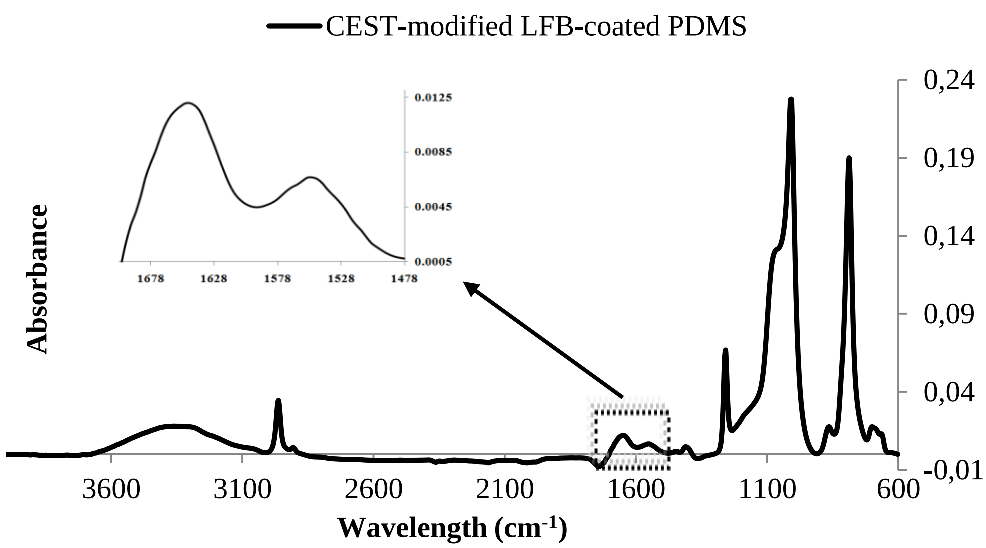

Fig. 24 The IR spectrum of (a) CEST-modified (b) CEST-modified LFB-coated PDMS

Table 8 PDMS surfaces before and after peptide conjugation with peak assignments [213-217]

Assignments	Pristine PDMS	UDA-modified LFB-coated PDMS	CEST-modified LFB-coated PDMS
NH stretching	-	3281	3360
Methyl CH	2963	2926	2963
Amide I	-	1637	1649
Amide II	-	1538	1552
$\delta(CH_3)$	-	1459	-
CH_3 asymmetric deformation	1411	1406	1409
CH_3 symmetric deformation	1258	1259	1259
Si-O-Si asymmetric stretching	1009	1007	1008
Si-C stretching	863	864	863
Si-$(CH_3)_2$	788	787	788
Surface	697	698	698

Table 9 shows how static water contact angle (WCA) values of the samples do change gradually from hydrophobic/hydrophilic behavior with respect to surface modifications. Pristine PDMS surfaces are obviously hydrophobic, demonstrating WCA of 102°. Meanwhile, oxygen-plasma treated PDMS surfaces show significant increase in hydrophilicity with a WCA of 9°, indeed water drop almost completely wetted the surface. The WCA of carboxylic acid terminated PDMS surfaces such as UDA-modified and CEST-modified PDMS were measured as 66° and 85°, respectively. A further decrease in contact angle upon LFB conjugation on PDMS surfaces was also observed, with WCA values as 57° for UDA-modified and 59° for CEST-modified PDMS.

Table 9 Water contact angles (WCA) of pristine PDMS and treated/modified PDMS surfaces

Sample	**WCA (°)**
Pristine PDMS	102
O_2 plasma-treated PDMS	9
UDA-modified PDMS	66
CEST-modified PDMS	85
UDA-modified LFB-coated PDMS	57
CEST-modified LFB-coated PDMS	59

For the purpose of exploring surface topography of the samples, confocal microscopy was utilized. Fig.24a demonstrates the surface of pristine PDMS, with bubble-like features which might be occurred during curing of the PDMS rubber. However, Fig.24b and Fig.24d shows LFB conjugated PDMS surfaces which seemed to be smoother following the surface coverage with the peptide. Bubble-like features are not as easily resolved as in the previous image. The difference between uncoated and LFB coated PDMS surfaces clearly appears in Fig.24c where the left part of the image exhibits uncoated PDMS looking rougher than LFB coated region at the right part. Besides, surface features of substrates were also visualized under SEM. As shown in Fig.25, PDMS surfaces have some scale formations in different sizes. Fig.25a also presents fine crack development between the scales on the surface of pristine PDMS. In Fig.25b and Fig.25c, these cracks seem to be wider following the oxygen plasma treatment which is done before surface modifications. However, the largest cracks were noticed in UDA-modified LFB coated surfaces. We suspect that this feature might happen because of high treatment temperature at around 80 °C which might have caused widening of cracks due to thermal stresses.

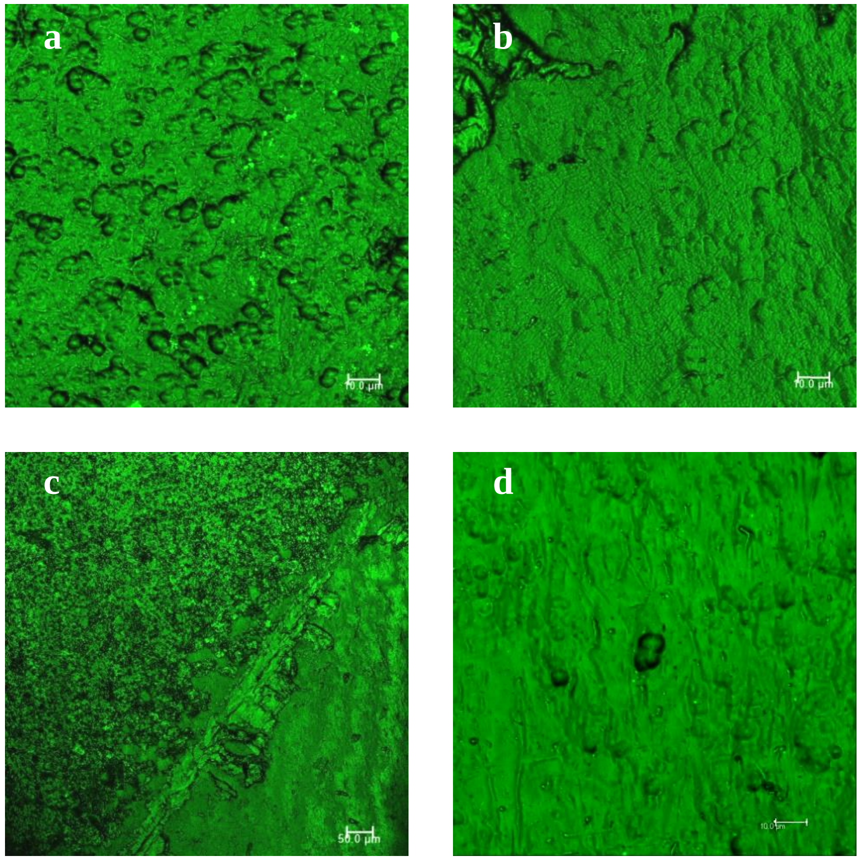

Fig. 25 Surface topography of (a) pristine PDMS (b) UDA-modified LFB coated PDMS (c) interface between uncoated and UDA-modified LFB coated PDMS (d) CEST-modified LFB coated PDMS

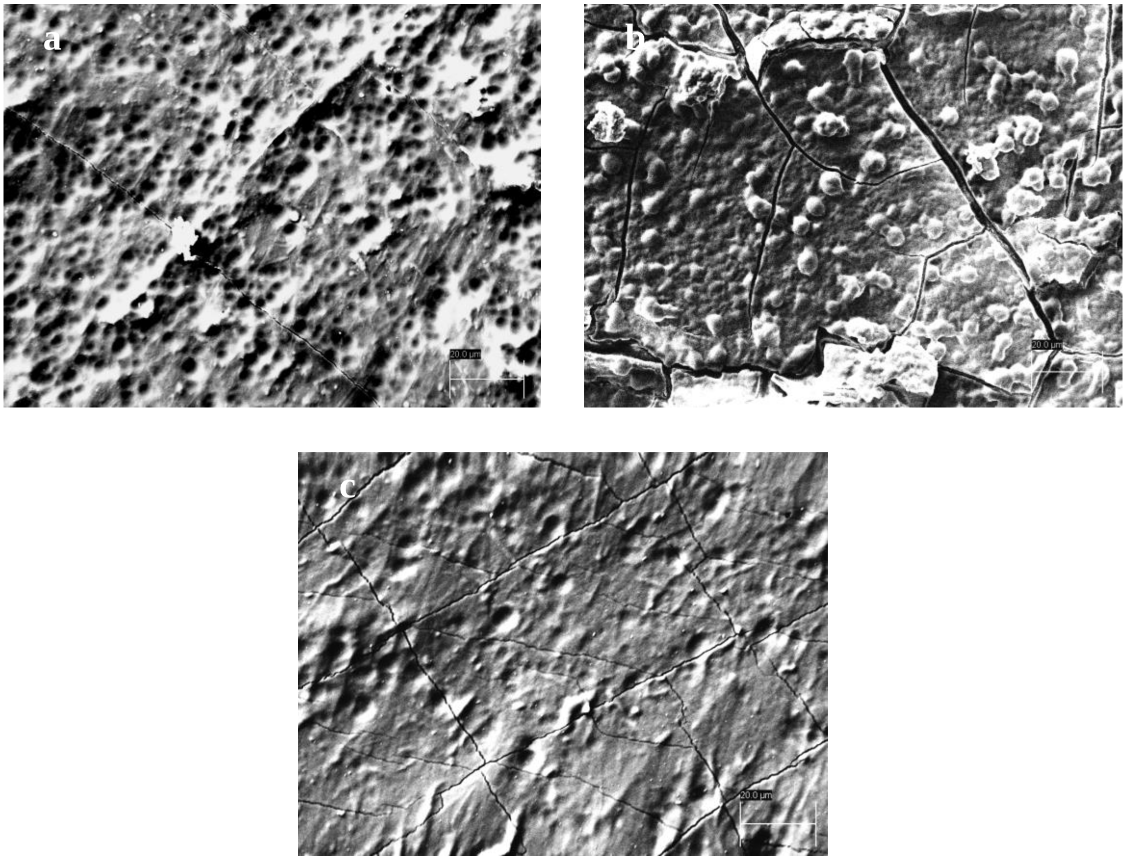

Fig. 26 SEM micrographs of (a) pristine PDMS (b) UDA-modified LFB coated PDMS (c) CEST-modified LFB coated PDMS

Fig.26 explicates the amount of bacterial colonies occurred on PDMS samples following *S. epidermidis* and *P. aeruginosa* exposure for 4 h. According to the results of *S. epidermidis* adhesion tests, UDA-modified LFB coated PDMS revealed a 98% reduction in bacterial colonization whereas CEST-modified LFB coated surfaces showed no significant change in bacteria amount. Experiments performed with *P. aeruginosa* demonstrated a notable decrease in the number of bacteria around 62% on UDA-modified LFB coated PDMS compared to pristine one. On the other hand, we reported a considerable rise in *P. aeruginosa* colonies on CEST-modified LFB coated surfaces, where the bacterial adhesion increased about 77%. Moreover, SEM micrographs in

Fig.27 also confirm the data obtained in bacterial adhesion tests. As seen in figure, the least bacterial adhesion was observed in UDA-modified LFB coated PDMS surfaces.

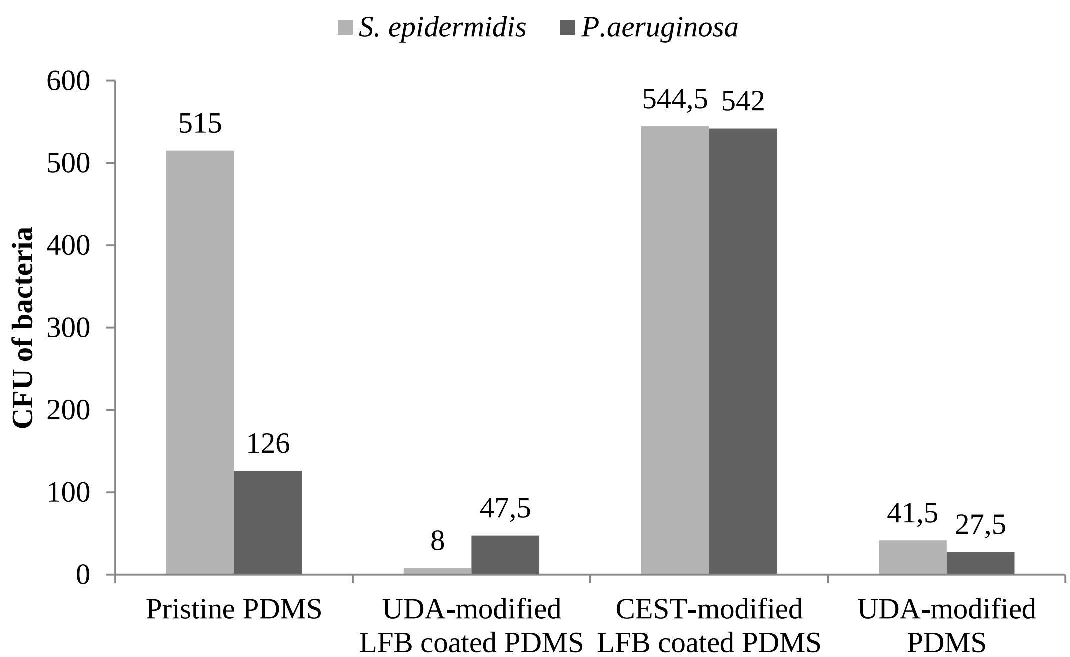

Fig. 27 The quantity of bacteria colonies after 4 h incubation on PDMS samples

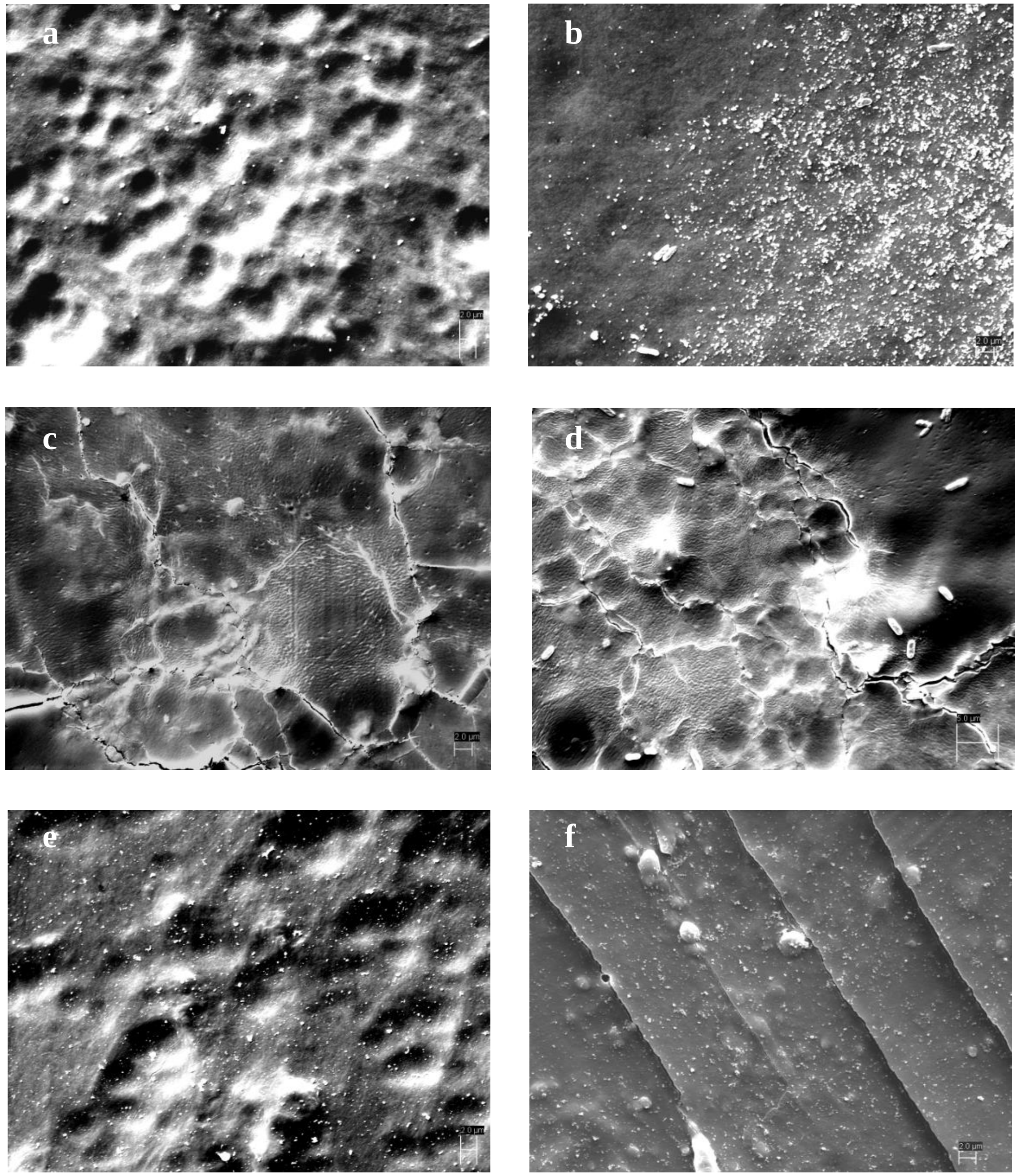

Fig. 28 SEM micrographs of S. epidermidis (left) and P. aeruginosa (right) on (a) (b) pristine PDMS (c) (d) UDA-modified LFB coated PDMS (e) (f) CEST-modified LFB coated PDMS

Antimicrobial peptides (AMPs), naturally part of our innate defense mechanisms, exert a wide range of antibacterial, antifungal and antiviral activity. Here we report the antibacterial performance of LFB when it is covalently grafted on biomedical grade PDMS surfaces. LFB_{20-25} fragment which is sequenced as RRWQWR (Arg-Arg-Trp-Gln-Trp-Arg), is generally accepted as the antimicrobial active core of LFB [166, 218-220]. This motif in lactoferrin-derived peptide consists of three positively charged (arginine) and two hydrophobic (tryptophan) amino acids [180]. Due to the presence of high amount of net positive charge (+8) and hydrophobic residues, this chain is speculated to be responsible for LCB's potential antibacterial activity [33, 176, 180, 221, 222]. These highly positively charged peptides may interact with negatively charged biological membranes [166]. Thus, the antibacterial effect of LFB is based on its performance of releasing of polysaccharide material from bacterial outer layer which may end up with disintegration of cytoplasmic membrane permeability in the case of gram (-) bacteria [223-225]. Following this destabilization, it blocks macromolecular biosynthesis and eventually results in cell death [48, 226]. In spite of lipopolysaccharides, they attack on lipoteichoic and teichoic acids of gram (+) bacteria [180].

According to bacterial adhesion tests performed for 4 h with *S. epidermidis* and *P. aeruginosa*, we assessed remarkable decrease in the amount of bacterial strains on UDA-modified LFB coated PDMS surface compared to pristine one. These results imply that LFB following chemical grafting via its lysine groups can retain its antibacterial activity, particularly if PDMS samples are modified by UDA. Furthermore, covalently bound peptide may show long-term peptide stability and debilitate their toxicity compared to release- or leach based applications [33]. At this stage, we also needed to examine the lone effect of UDA which is especially well-reputed with its antifungal action [227-229]. Compared to only UDA-modified PDMS surfaces, LFB coated ones demonstrated around 81% more potential antibacterial performance against *S. epidermidis*. Nonetheless, we did not detect the same trend in *P. aeruginosa* adhesion. With reference to UDA-modified LFB coated PDMS, just UDA-modified PDMS samples exhibited a notable reduction in the quantity of gram (-) bacteria around 60%.

In contrast to UDA-modified LFB coated PDMS surfaces, we did not record any antibacterial potency on CEST-modified LFB coated surfaces. For the aim of carrying out silanization process to mediate carboxyl-group immobilization on PDMS surfaces, we applied O_2 plasma treatment to generate OH groups. However, these OH bonds might not be intense and stable enough to create carboxylic acid groups via silane-coupling compounds. Though we observed considerable decrease in water contact angle after O_2 plasma exposure on surfaces, we noticed that contact angle reverted back close to its original value after rinsing the surface with water. Hence, we concluded that there exist very little amount of CEST on the surface which might not allow adequate peptide conjugation on PDMS surfaces. The decrease in contact angle value also depends on the plasma power and exposure time [189]. As a result, in our future work we consider to treat PDMS surfaces with higher plasma power than 100 W for CEST-modification. In spite of several benefits of PDMS, its major drawback is the recovery of its hydrophobicity in short-period of time. Owen's group stated this phenomenon with some explanations [230]:

a) Reorientation of surface polar groups (OH) into bulk polymer
b) Reorientation of nonpolar groups (CH_3) from the bulk phase to the surface
c) Cracks due to the formation of SiO_x structure which generates voids for mobile free PDMS chains from the bulk to the surface
d) Loss of volatile oxygen rich species into the atmosphere
e) Diffusion of low-molecular-weight oligomers and additives from bulk phase to the surface

3.4 Conclusion

Experiments showed that UDA-modified LFB coated silicone rubber surfaces had exhibited notable reduction in both *S. epidermidis* and *P. aeruginosa* adhesion regarding pristine rubber. As a result, this reduction is specifically associated with the successful conjugation of cationic peptide brushes on PDMS surfaces via carbodiimide reaction in the presence of NHS. We conclude that LFB not only appropriately grafted, but also its antibacterial motif RRWQWR is still available to demonstrate its bactericidal action even after immobilization. On the other hand, we did not observe the same behavior on CEST-modified LFB coated PDMS. As a matter of fact, what we deduced from ATR-FTIR data is there exists very little amount of CEST on the surface which might not allow adequate peptide conjugation on PDMS surfaces. Hence, UDA-modified LFB conjugated PDMS results are encouraging evidence supporting cationic peptides as an alternative promising approach to create safe antibacterial surfaces on polymer-based long-term biomedical devices, granting that these cationic peptides do not trigger any bacteria mutations as their other alternatives still in use commercially.

CHAPTER 4

4. CONCLUSION AND FUTURE WORK

In the context of these researches, we aimed to develop inorganic and organic smart surfaces for antibacterial applications. First, we investigated the bacteriostatic effect of BN thin film coatings with different crystallographic morphologies on 316L grade steel. In the light of this study, we stated how the spatial arrangement of atoms in crystallographic structure influences the bacterial adhesion on substrate surfaces. In addition, we assessed the anti-biofouling properties of LFB immobilized biomedical grade PDMS surfaces. Here we report successful conjugation of cationic peptides and their deterrent effect against bacterial adhesion while preserving their lethal activity towards pathogens. In the future work, we are proposing to repeat the experiments for 24 h incubation periods in order to discern long-term anti-microbial activity of LFB. One important investigation will be to determine the viability of the attaching microorganisms. We are also planning to test silicone rubber surfaces against C. *albicans.* Due to time constraints, cytotoxicity tests of UDA and CEST modification as well as LFB are not done yet. Particularly UDA is a medicinal chemical used in low quantities for treatment of fungal infections like athlete's foot disease. In case that we encounter some cyctoxicity with UDA modified samples against mammalian cells, we will alternatively consider repeating CEST modification either with a high power O_2 plasma instrument or OH functionalized PDMS rubber to create LFB modified surfaces without UDA grafts.

REFERENCES

1. Cowan, M.K. and K.P. Talaro, *Microbiology: A systems approach*. 2006, New York: McGraw-Hill
2. Prescott, L.M., J.P. Harley, and D.A. Klein, *Microbiology*. 5th ed. 2002: McGraw-Hill
3. An, Y.H. and R.J. Friedman, *Concise review of mechanisms of bacterial adhesion to biomaterial surfaces.* J Biomed Mater Res, 1998. **43**(3): p. 338-48.
4. Costerton, J.W., P.S. Stewart, and E.P. Greenberg, *Bacterial biofilms: a common cause of persistent infections.* Science, 1999. **284**(5418): p. 1318-22.
5. Francolini, I. and G. Donelli, *Prevention and control of biofilm-based medical-device-related infections.* FEMS Immunology & Medical Microbiology, 2010. **59**(3): p. 227-238.
6. Habash, M. and G. Reid, *Microbial biofilms: their development and significance for medical device-related infections.* J Clin Pharmacol, 1999. **39**(9): p. 887-98.
7. Ratner, B.D., et al., *Biomaterials Science: An Introduction to Materials in Medicine*. 1996: Elsevier.
8. Guzman, M., J. Dille, and S. Godet, *Synthesis and antibacterial activity of silver nanoparticles against gram-positive and gram-negative bacteria.* Nanomedicine, 2012. **8**(1): p. 37-45.
9. Hajipour, M.J., et al., *Antibacterial properties of nanoparticles.* Trends in Biotechnology, 2012. **30**(10): p. 499-511.
10. Siqueira, J.F., Jr. and H.P. Lopes, *Mechanisms of antimicrobial activity of calcium hydroxide: a critical review.* Int Endod J, 1999. **32**(5): p. 361-9.
11. Powers, J.P. and R.E. Hancock, *The relationship between peptide structure and antibacterial activity.* Peptides, 2003. **24**(11): p. 1681-91.
12. Carlson, G.A., et al., *Bacteriostatic properties of biomatrices against common orthopaedic pathogens.* Biochem Biophys Res Commun, 2004. **321**(2): p. 472-8.
13. Banerjee, I., R.C. Pangule, and R.S. Kane, *Antifouling coatings: recent developments in the design of surfaces that prevent fouling by proteins, bacteria, and marine organisms.* Adv Mater, 2011. **23**(6): p. 690-718.

14. Cassinelli, C., et al., *Evaluation of interfacial properties of hyaluronan coated poly(methylmethacrylate) intraocular lenses.* J Biomater Sci Polym Ed, 2000. **11**(9): p. 961-77.
15. John, T., et al., *Antibiotic pretreatment of hydrogel ureteral stent.* J Endourol, 2007. **21**(10): p. 1211-6.
16. Appelgren, P., et al., *Surface heparinization of central venous catheters reduces microbial colonization in vitro and in vivo: results from a prospective, randomized trial.* Crit Care Med, 1996. **24**(9): p. 1482-9.
17. Russell, P.B., et al., *Staphylococcal adherence to polyvinyl chloride and heparin-bonded polyurethane catheters is species dependent and enhanced by fibronectin.* J Clin Microbiol, 1987. **25**(6): p. 1083-7.
18. Berendjchi, A., R. Khajavi, and M.E. Yazdanshenas, *Fabrication of superhydrophobic and antibacterial surface on cotton fabric by doped silica-based sols with nanoparticles of copper.* Nanoscale Res Lett, 2011. **6**(1): p. 6-594.
19. Abdel-Aziz, M.S., et al., *Antioxidant and antibacterial activity of silver nanoparticles biosynthesized using Chenopodium murale leaf extract.* Journal of Saudi Chemical Society, 2013(0).
20. Baba, K., et al., *Preparation and Properties of Ag-Containing Diamond-Like Carbon Films by Magnetron Plasma Source Ion Implantation.* Advances in Materials Science and Engineering, 2012. **2012**: p. 5.
21. Chiang, W.-C., et al., *Influence of silver additions to type 316 stainless steels on bacterial inhibition, mechanical properties, and corrosion resistance.* Materials Chemistry and Physics, 2010. **119**(1–2): p. 123-130.
22. Davies, R.L. and S.F. Etris, *The development and functions of silver in water purification and disease control.* Catalysis Today, 1997. **36**(1): p. 107-114.
23. Jung, W.K., et al., *Antibacterial activity and mechanism of action of the silver ion in Staphylococcus aureus and Escherichia coli.* Appl Environ Microbiol, 2008. **74**(7): p. 2171-8.
24. Morones, J.R., et al., *The bactericidal effect of silver nanoparticles.* Nanotechnology, 2005. **16**(10): p. 2346-53.
25. Pal, S., Y.K. Tak, and J.M. Song, *Does the antibacterial activity of silver nanoparticles depend on the shape of the nanoparticle? A study of the Gram-negative bacterium Escherichia coli.* Appl Environ Microbiol, 2007. **73**(6): p. 1712-20.
26. Prabhu, S. and E. Poulose, *Silver nanoparticles: mechanism of antimicrobial action, synthesis, medical applications, and toxicity effects.* International Nano Letters, 2012. **2**(1): p. 1-10.
27. Shahverdi, A.R., et al., *Synthesis and effect of silver nanoparticles on the antibacterial activity of different antibiotics against Staphylococcus aureus and Escherichia coli.* Nanomedicine: Nanotechnology, Biology and Medicine, 2007. **3**(2): p. 168-171.
28. Sondi, I. and B. Salopek-Sondi, *Silver nanoparticles as antimicrobial agent: a case study on E. coli as a model for Gram-negative bacteria.* Journal of Colloid and Interface Science, 2004. **275**(1): p. 177-182.

29. Richards, R.M., H.A. Odelola, and B. Anderson, *Effect of silver on whole cells and spheroplasts of a silver resistant Pseudomonas aeruginosa.* Microbios, 1984. **39**(157-158): p. 151-7.
30. Bailey, P.J., et al., *Boron-containing antibacterial agents: effects on growth and morphology of bacteria under various culture conditions.* Antimicrob Agents Chemother, 1980. **17**(4): p. 549-53.
31. Bursali, E.A., et al., *Synthesis, characterization and in vitro antimicrobial activities of boron/starch/polyvinyl alcohol hydrogels.* Carbohydrate Polymers, 2011. **83**(3): p. 1377-1383.
32. Costa, F., et al., *Covalent immobilization of antimicrobial peptides (AMPs) onto biomaterial surfaces.* Acta Biomater, 2011. **7**(4): p. 1431-40.
33. Costa, F., et al., *Characterization of hLF1-11 immobilization onto chitosan ultrathin films, and its effects on antimicrobial activity.* Acta Biomater, 2014.
34. Jenssen, H., P. Hamill, and R.E. Hancock, *Peptide antimicrobial agents.* Clin Microbiol Rev, 2006. **19**(3): p. 491-511.
35. Kazemzadeh-Narbat, M., et al., *Antimicrobial peptides on calcium phosphate-coated titanium for the prevention of implant-associated infections.* Biomaterials, 2010. **31**(36): p. 9519-26.
36. Willcox, M.D.P., et al., *A novel cationic-peptide coating for the prevention of microbial colonization on contact lenses.* Journal of Applied Microbiology, 2008. **105**(6): p. 1817-1825.
37. Guggenbichler, J.P., et al., *Incidence and clinical implication of nosocomial infections associated with implantable biomaterials - catheters, ventilator-associated pneumonia, urinary tract infections.* GMS Krankenhhyg Interdiszip, 2011. **6**(1): p. 15.
38. Pereni, C.I., et al., *Surface free energy effect on bacterial retention.* Colloids and Surfaces B: Biointerfaces, 2006. **48**(2): p. 143-147.
39. Liu, C., et al., *Reduction of bacterial adhesion on modified DLC coatings.* Colloids and Surfaces B: Biointerfaces, 2008. **61**(2): p. 182-187.
40. Donlan, R.M., *Biofilms and device-associated infections.* Emerg Infect Dis, 2001. **7**(2): p. 277-81.
41. Vertes, A., V. Hitchins, and K.S. Phillips, *Analytical Challenges of Microbial Biofilms on Medical Devices.* Analytical Chemistry, 2012. **84**(9): p. 3858-3866.
42. Arnold, J.W. and G.W. Bailey, *Surface finishes on stainless steel reduce bacterial attachment and early biofilm formation: scanning electron and atomic force microscopy study.* Poult Sci, 2000. **79**(12): p. 1839-45.
43. Bollen, C.M.L., P. Lambrechts, and M. Quirynen, *Comparison of surface roughness of oral hard materials to the threshold surface roughness for bacterial plaque retention: A review of the literature.* Dental Materials, 1997. **13**(4): p. 258-269.
44. Bollen, C.M.L., et al., *The influence of abutment surface roughness on plaque accumulation and peri-implant mucositis.* Clinical Oral Implants Research, 1996. **7**(3): p. 201-211.
45. Boulangé-Petermann, L., J. Rault, and M.N. Bellon-Fontaine, *Adhesion of streptococcus thermophilus to stainless steel with different surface topography and roughness.* Biofouling, 1997. **11**(3): p. 201-216.

46. Fan, Y.W., et al., *Culture of neural cells on silicon wafers with nano-scale surface topograph.* Journal of Neuroscience Methods, 2002. **120**(1): p. 17-23.
47. Flint, S.H., J.D. Brooks, and P.J. Bremer, *Properties of the stainless steel substrate, influencing the adhesion of thermo-resistant streptococci.* Journal of Food Engineering, 2000. **43**(4): p. 235-242.
48. Hilbert, L.R., et al., *Influence of surface roughness of stainless steel on microbial adhesion and corrosion resistance.* International Biodeterioration & Biodegradation, 2003. **52**(3): p. 175-185.
49. Medilanski, E., et al., *Influence of the Surface Topography of Stainless Steel on Bacterial Adhesion.* Biofouling, 2002. **18**(3): p. 193-203.
50. Wu, Y., et al., *Differential response of Staphylococci and osteoblasts to varying titanium surface roughness.* Biomaterials, 2011. **32**(4): p. 951-960.
51. Zhou, H., et al., *Investigation into the antibacterial property of carbon films.* Diamond and Related Materials, 2008. **17**: p. 1416-1419.
52. De Prijck, K., et al., *Candida albicans biofilm formation on peptide functionalized polydimethylsiloxane.* Biofouling, 2010. **26**(3): p. 269-75.
53. Bos, R., et al., *Retention of bacteria on a substratum surface with micro-patterned hydrophobicity.* FEMS Microbiology Letters, 2000. **189**(2): p. 311-315.
54. MacKintosh, E.E., et al., *Effects of biomaterial surface chemistry on the adhesion and biofilm formation of Staphylococcus epidermidis in vitro.* Journal of Biomedical Materials Research Part A, 2006. **78A**(4): p. 836-842.
55. Sodhi, R.N.S., V.P. Sahi, and M.W. Mittelman, *Application of electron spectroscopy and surface modification techniques in the development of anti-microbial coatings for medical devices.* Journal of Electron Spectroscopy and Related Phenomena, 2001. **121**(1-3): p. 249-264.
56. Tang, H., et al., *Influence of silicone surface roughness and hydrophobicity on adhesion and colonization of Staphylococcus epidermidis.* Journal of Biomedical Materials Research Part A, 2009. **88A**(2): p. 454-463.
57. Bos, R., H.C. van der Mei, and H.J. Busscher, *Physico-chemistry of initial microbial adhesive interactions--its mechanisms and methods for study.* FEMS Microbiol Rev, 1999. **23**(2): p. 179-230.
58. Li, B. and B.E. Logan, *Bacterial adhesion to glass and metal-oxide surfaces.* Colloids and Surfaces B: Biointerfaces, 2004. **36**(2): p. 81-90.
59. Terada, A., et al., *The effect of surface charge property on Escherichia coli initial adhesion and subsequent biofilm formation.* Biotechnol Bioeng, 2012. **109**(7): p. 1745-54.
60. van Loosdrecht, M.C., et al., *Electrophoretic mobility and hydrophobicity as a measured to predict the initial steps of bacterial adhesion.* Appl Environ Microbiol, 1987. **53**(8): p. 1898-901.
61. Weerkamp, A.H., H.M. Uyen, and H.J. Busscher, *Effect of zeta potential and surface energy on bacterial adhesion to uncoated and saliva-coated human enamel and dentin.* J Dent Res, 1988. **67**(12): p. 1483-7.
62. Harden, V.P. and J.O. Harris, *The isoelectric point of bacterial cells.* J Bacteriol, 1953. **65**(2): p. 198-202.

63. Hogt, A.H., J. Dankert, and J. Feijen, *Adhesion of Staphylococcus epidermidis and Staphylococcus saprophyticus to a hydrophobic biomaterial.* J Gen Microbiol, 1985. **131**(9): p. 2485-91.
64. Fletcher, M. and G.I. Loeb, *Influence of substratum characteristics on the attachment of a marine pseudomonad to solid surfaces.* Appl Environ Microbiol, 1979. **37**(1): p. 67-72.
65. Ahmad, S., et al., *Urethane modified boron filled polyesteramide: a novel anti-microbial polymer from a sustainable resource.* European Polymer Journal, 2004. **40**(9): p. 2097-2104.
66. Dion, I., et al., *Physico-chemistry and cytotoxicity of ceramics. Part II. Cytotoxicity of ceramics.* Journal of Materials Science: Materials in Medicine, 1994. **5**(1): p. 18-24.
67. Koga, K., et al., *Cytotoxic evaluation of cubic boron nitride in human origin cultured cells.* Toxicology in Vitro, 2006. **20**(8): p. 1370-1377.
68. Lattemann, M., et al., *Stress reduction in nanocomposite coatings consisting of hexagonal and cubic boron nitride.* Surface and Coatings Technology, 2006. **200**(22-23): p. 6459-6464.
69. Ye, J., U. Rothhaar, and H. Oechsner, *Conditions for the formation of cubic boron nitride films by r.f. magnetron sputtering.* Surface and Coatings Technology, 1998. **105**(1–2): p. 159-164.
70. Kaftanoglu, B. and N. Dokmetas, *An environmentally friendly method of cutting and forming of materials by c-BN coated tools*, in *10th Global Conference*. 2012: Istanbul, Turkey.
71. Cesur, H. and B. Kaftanoglu, *An experimental study about cBN formation for cutting tools*, in *5th International Conference and Exhibition on Design and Production of Machines and Dies/Molds*. 2009: Aydin, Turkey.
72. Kulisch, W. and R. Freudenstein, *Deposition of thick cubic boron nitride films - Mechanisms and concepts.* Thin Solid Films, 2007. **516**: p. 216-222.
73. Uhlmann, E., J.A.O. Fuentes, and M. Keunecke, *Machining of high performance workpiece materials with CBN coated cutting tools.* Thin Solid Films, 2009. **518**(5): p. 1451-1454.
74. Trigwell, S. and G. Selvaduray, *Effect of surface treatment on the surface characteristics of AISI 316L stainless steel*, in *Proc. Materials & Processes for Medical Devices Conf. ASM Int.* 2005: (Boston, MA) p. 14-6.
75. Rivardo, F., et al., *Synergistic effect of lipopeptide biosurfactant with antibiotics against Escherichia coli CFT073 biofilm.* International Journal of Antimicrobial Agents, 2011. **37**(4): p. 324-331.
76. Mattox, D.M., ed. *Handbook of Physical Vapor Deposition (PVD) Processing*. 2. ed. 2010, Oxford: Elsevier Science. 792.
77. Mellor, B.G., ed. *Surface Coatings for Protection against Wear*. 2006, Woodhead Publishing Limited: Cambridge, UK. 429.
78. Suryanarayana, C., *Non-equilibrium processing of materials*. 1999, Pergamon: Amsterdam p. 438.
79. Mirkarimi, P.B., K.F. McCarty, and D.L. Medlin, *Review of advances in cubic boron nitride film synthesis.* Materials Science and Engineering: R: Reports, 1997. **21**(2): p. 47-100.

80. ThermoNicolet. *Introduction to Fourier Transform Infrared Spectrometry*. 2001.
81. Griffiths, P.R. and J.A. De Haseth, *Fourier Transform Infrared Spectrometry*. 2. ed. 2007, Hoboken, New Jersey: John Wiley & Sons, Inc. 536.
82. Smith, B.C., *Fundamentals of Fourier Transform Infrared Spectroscopy*. 2. ed. 2011, Boca Raton, FL: CRC Press, Taylor & Francis Group. 182.
83. Tolstoy, V.P., I.V. Chernyshova, and V.A. Skryshevsky, *Handbook of infrared spectroscopy of ultrathin films*. 2003, Hoboken, New Jersey: John Wiley & Sons, Inc.
84. Chu, P.K. and L. Li, *Characterization of amorphous and nanocrystalline carbon films.* Materials Chemistry and Physics, 2006. **96**(2–3): p. 253-277.
85. Bowen, W.R. and N. Hilal, *Atomic Force Microscopy in Process Engineering: An Introduction to AFM for Improved Processes and Products*. 2009: Butterworth-Heinemann. 304.
86. Kaupp, G., *Atomic Force Microscopy, Scanning Nearfield Optical Microscopy and Nanoscratching: Application to Rough and Natural Surfaces*. 2006: Springer. 304.
87. Smith, K.C.A. and C.W. Oatley, *The scanning electron microscope and its fields of application.* British Journal of Applied Physics, 1955. **6**(11): p. 391.
88. Reed, S.J.B., *Electron Microprobe Analysis and Scanning Electron Microscopy in Geology*. 2005: Cambridge University Press.
89. Egerton, F.R., *Physical Principles of Electron Microscopy: An Introduction to TEM, SEM, and AEM*. 2005: Springer Science+Business Media, Inc. 202.
90. Mittal, K.L., *Contact Angle, Wettability and Adhesion, Volume 3*. 2003, VSP - An imprint of BRILL. p. 519.
91. Israelachvili, J.N., *Intermolecular and Surface Forces*. 3. ed. 2011: Academic Press. 710.
92. Young, T., *An Essay on the Cohesion of Fluids.* Philosophical Transactions of the Royal Society of London, 1805. **95**: p. 65-87.
93. Zisman, W.A., *Relation of the Equilibrium Contact Angle to Liquid and Solid Constitution*, in *Contact Angle, Wettability, and Adhesion*. 1964, AMERICAN CHEMICAL SOCIETY. p. 1-51.
94. Owens, D.K. and R.C. Wendt, *Estimation of the surface free energy of polymers.* Journal of Applied Polymer Science, 1969. **13**(8): p. 1741-1747.
95. Beloin, C., A. Roux, and J.M. Ghigo, *Escherichia coli biofilms.* Curr Top Microbiol Immunol, 2008. **322**: p. 249-89.
96. Ren, D., et al., *Differential gene expression for investigation of Escherichia coli biofilm inhibition by plant extract ursolic acid.* Appl Environ Microbiol, 2005. **71**(7): p. 4022-34.
97. Albayrak, N., D. Biriken, and H. Ozenci, *Investigation of the bactericidal effect of urinary epithelial cells against different doses of Escherichia coli.* Mikrobiyol Bul, 2006. **40**(3): p. 195-200.
98. Gimeno, S., J.C. Muñoz, and A. Lousa, *Adherence experiments on cBN films.* Diamond and Related Materials, 1998. **7**(6): p. 853-857.
99. Jäger, S., K. Bewilogua, and C.P. Klages, *Infrared spectroscopic investigations on h-BN and mixed h/c-BN thin films.* Thin Solid Films, 1994. **245**(1–2): p. 50-54.

100. Yu, L., et al., *In situ FTIR investigation on phase transformations in BN nanoparticles.* Chinese Science Bulletin, 2005. **50**(24): p. 2827-2831.
101. Weidner, S., et al., *Extension of the cubic boron nitride thin film growth phase diagram.* Diamond and Related Materials, 2012. **22**(0): p. 88-91.
102. Yang, H., A. Chen, and F. Qiu, *Cubic boron nitride film residual compressive stress relaxation by post annealing.* Diamond and Related Materials, 2011. **20**(8): p. 1179-1182.
103. Hacking, S.A., et al., *A physical vapor deposition method for controlled evaluation of biological response to biomaterial chemistry and topography.* J Biomed Mater Res A, 2007. **82**(1): p. 179-87.
104. Vanhaecke, E., et al., *Kinetics of Pseudomonas aeruginosa adhesion to 304 and 316-L stainless steel: role of cell surface hydrophobicity.* Appl Environ Microbiol, 1990. **56**(3): p. 788-95.
105. Cheong, W.C., P.H. Gaskell, and A. Neville, *Substrate effect on surface adhesion/crystallisation of calcium carbonate.* Journal of Crystal Growth, 2013. **363**(0): p. 7-21.
106. Größner-Schreiber, B., et al., *Focal adhesion contact formation by fibroblasts cultured on surface-modified dental implants: an in vitro study.* Clinical Oral Implants Research, 2006. **17**(6): p. 736-745.
107. Chen, L.-Y. and F. Chau-Nan Hong, *Surface tension studies of (Si, N)-containing diamond-like carbon films deposited by hexamethyldisilazane.* Diamond and Related Materials, 2003. **12**(3–7): p. 968-973.
108. Hod, O., *Graphite and Hexagonal Boron-Nitride have the Same Interlayer Distance. Why?* Journal of Chemical Theory and Computation, 2012. **8**(4): p. 1360-1369.
109. Boulange-Petermann, L., B. Baroux, and M.-N. Bellon-Fontaine, *The influence of metallic surface wettability on bacterial adhesion.* Journal of Adhesion Science and Technology, 1993. **7**(3): p. 221-230.
110. Ducker, W.A., T.J. Senden, and R.M. Pashley, *Measurement of forces in liquids using a force microscope.* Langmuir, 1992. **8**(7): p. 1831-1836.
111. William, A.D., J.S. Tim, and M.P. Richard, *Direct measurement of colloidal forces using an atomic force microscope.* Nature, 1991. **353**(6341): p. 239-241.
112. Butt, H.J., *Measuring electrostatic, van der Waals, and hydration forces in electrolyte solutions with an atomic force microscope.* Biophys J, 1991. **60**(6): p. 1438-44.
113. Hu, K., M. Brust, and A.J. Bard, *Characterization and Surface Charge Measurement of Self-Assembled CdS Nanoparticle Films.* Chemistry of Materials, 1998. **10**(4): p. 1160-1165.
114. Oliveira, R., *Understanding adhesion: A means for preventing fouling.* Experimental Thermal and Fluid Science, 1997. **14**(4): p. 316-322.
115. Chen, G. and S.L. Walker, *Role of Solution Chemistry and Ion Valence on the Adhesion Kinetics of Groundwater and Marine Bacteria.* Langmuir, 2007. **23**(13): p. 7162-7169.
116. Geesey, G.G., B. Wigglesworth-Cooksey, and K.E. Cooksey, *Influence of calcium and other cations on surface adhesion of bacteria and diatoms: A review.* Biofouling, 2000. **15**(1-3): p. 195-205.

117. Ueshima, M., et al., *Manipulation of bacterial adhesion and proliferation by surface charges of electrically polarized hydroxyapatite.* J Biomed Mater Res, 2002. **60**(4): p. 578-84.
118. Beveridge, T.J., *Role of cellular design in bacterial metal accumulation and mineralization.* Annu Rev Microbiol, 1989. **43**: p. 147-71.
119. Beveridge, T.J. and R.G. Murray, *Uptake and retention of metals by cell walls of Bacillus subtilis.* J Bacteriol, 1976. **127**(3): p. 1502-18.
120. Beveridge, T.J. and R.G. Murray, *Sites of metal deposition in the cell wall of Bacillus subtilis.* J Bacteriol, 1980. **141**(2): p. 876-87.
121. Stevik, T.K., et al., *Retention and removal of pathogenic bacteria in wastewater percolating through porous media: a review.* Water Res, 2004. **38**(6): p. 1355-67.
122. Petrescu, M. and M.-G. Balint, *Structure and properties modifications in boron nitride. Part I: Direct polymorphic transformations mechanisms.*
123. Hawser, S.P. and L.J. Douglas, *Biofilm formation by Candida species on the surface of catheter materials in vitro.* Infect Immun, 1994. **62**(3): p. 915-21.
124. Dohnt, K., et al., *An in vitro urinary tract catheter system to investigate biofilm development in catheter-associated urinary tract infections.* Journal of Microbiological Methods, 2011. **87**(3): p. 302-308.
125. Gristina, A.G., *Biomaterial-centered infection: microbial adhesion versus tissue integration.* Science, 1987. **237**(4822): p. 1588-95.
126. Nowatzki, P.J., et al., *Salicylic acid-releasing polyurethane acrylate polymers as anti-biofilm urological catheter coatings.* Acta Biomaterialia, 2012. **8**(5): p. 1869-1880.
127. Costerton, J.W., et al., *Bacterial biofilms in nature and disease.* Annu Rev Microbiol, 1987. **41**: p. 435-64.
128. Costerton, J.W., R.T. Irvin, and K.J. Cheng, *The bacterial glycocalyx in nature and disease.* Annu Rev Microbiol, 1981. **35**: p. 299-324.
129. Donlan, R.M. and J.W. Costerton, *Biofilms: survival mechanisms of clinically relevant microorganisms.* Clin Microbiol Rev, 2002. **15**(2): p. 167-93.
130. Zhao, X., et al., *Candida albicans Als3p is required for wild-type biofilm formation on silicone elastomer surfaces.* Microbiology, 2006. **152**(Pt 8): p. 2287-99.
131. Humblot, V., et al., *The antibacterial activity of Magainin I immobilized onto mixed thiols Self-Assembled Monolayers.* Biomaterials, 2009. **30**(21): p. 3503-12.
132. Lewis, K., *Riddle of biofilm resistance.* Antimicrob Agents Chemother, 2001. **45**(4): p. 999-1007.
133. Raad, II, et al., *Prevention of central venous catheter-related infections by using maximal sterile barrier precautions during insertion.* Infect Control Hosp Epidemiol, 1994. **15**(4 Pt 1): p. 231-8.
134. Zhang, L., J. Gowardman, and C.M. Rickard, *Impact of microbial attachment on intravascular catheter-related infections.* International Journal of Antimicrobial Agents, 2011. **38**(1): p. 9-15.
135. Parameswaran, R., et al., *Intravascular catheter-related infections in an Indian tertiary care hospital.* J Infect Dev Ctries, 2011. **5**(6): p. 452-8.

136. Dai, L., et al., *Staphylococcus epidermidis recovered from indwelling catheters exhibit enhanced biofilm dispersal and self-renewal through downregulation of agr.* BMC Microbiology, 2012. **12**(102): p. 246-250.
137. Elliott, T.S., et al., *Novel approach to investigate a source of microbial contamination of central venous catheters.* Eur J Clin Microbiol Infect Dis, 1997. **16**(3): p. 210-3.
138. Etienne, O., et al., *Multilayer polyelectrolyte films functionalized by insertion of defensin: a new approach to protection of implants from bacterial colonization.* Antimicrob Agents Chemother, 2004. **48**(10): p. 3662-9.
139. Raad, I., *Intravascular-catheter-related infections.* Lancet, 1998. **351**(9106): p. 893-8.
140. van Eck van der Sluijs, A., et al., *Bacteremic complications of intravascular catheter tip colonization with Gram-negative micro-organisms in patients without preceding bacteremia.* European Journal of Clinical Microbiology & Infectious Diseases, 2012. **31**(6): p. 1027-1033.
141. Bryers, J.D., *Medical biofilms.* Biotechnol Bioeng, 2008. **100**(1): p. 1-18.
142. Ha, U.S. and Y.H. Cho, *Catheter-associated urinary tract infections: new aspects of novel urinary catheters.* Int J Antimicrob Agents, 2006. **28**(6): p. 485-90.
143. Hola, V., T. Peroutkova, and F. Ruzicka, *Virulence factors in Proteus bacteria from biofilm communities of catheter-associated urinary tract infections.* FEMS Immunology and Medical Microbiology, 2012. **65**(2): p. 343-349.
144. Stamm, W.E., *Catheter-associated urinary tract infections: epidemiology, pathogenesis, and prevention.* Am J Med, 1991. **91**(3B): p. 65S-71S.
145. Warren, J.W., *Catheter-associated urinary tract infections.* International Journal of Antimicrobial Agents, 2001. **17**(4): p. 299-303.
146. Djeribi, R., et al., *Characterization of bacterial biofilms formed on urinary catheters.* American Journal of Infection Control, 2012. **40**(9): p. 854-859.
147. Stickler, D.J., *Bacterial biofilms and the encrustation of urethral catheters.* Biofouling, 1996. **9**(4): p. 293-305.
148. Darouiche, R.O., et al., *A comparison of two antimicrobial-impregnated central venous catheters. Catheter Study Group.* N Engl J Med, 1999. **340**(1): p. 1-8.
149. Hanna, H., et al., *Long-term silicone central venous catheters impregnated with minocycline and rifampin decrease rates of catheter-related bloodstream infection in cancer patients: a prospective randomized clinical trial.* J Clin Oncol, 2004. **22**(15): p. 3163-71.
150. Reid, G., et al., *Effects of ciprofloxacin, norfloxacin, and ofloxacin on in vitro adhesion and survival of Pseudomonas aeruginosa AK1 on urinary catheters.* Antimicrob Agents Chemother, 1994. **38**(7): p. 1490-5.
151. Flemming, R.G., et al., *Bacterial colonization of functionalized polyurethanes.* Biomaterials, 2000. **21**(3): p. 273-81.
152. Gottenbos, B., et al., *In vitro and in vivo antimicrobial activity of covalently coupled quaternary ammonium silane coatings on silicone rubber.* Biomaterials, 2002. **23**(6): p. 1417-23.
153. Klibanov, A.M., *Permanently microbicidal materials coatings.* Journal of Materials Chemistry, 2007. **17**(24): p. 2479-2482.

154. Lee, S.B., et al., *Permanent, nonleaching antibacterial surfaces. 1. Synthesis by atom transfer radical polymerization.* Biomacromolecules, 2004. **5**(3): p. 877-82.
155. Chung, D., S.E. Papadakis, and K.L. Yam, *Evaluation of a polymer coating containing triclosan as the antimicrobial layer for packaging materials.* International Journal of Food Science & Technology, 2003. **38**(2): p. 165-169.
156. Sunada, K., T. Watanabe, and K. Hashimoto, *Studies on photokilling of bacteria on TiO2 thin film.* Journal of Photochemistry and Photobiology A: Chemistry, 2003. **156**(1–3): p. 227-233.
157. Flowers, R.H., 3rd, et al., *Efficacy of an attachable subcutaneous cuff for the prevention of intravascular catheter-related infection. A randomized, controlled trial.* Jama, 1989. **261**(6): p. 878-83.
158. Ahearn, D.G., et al., *Effects of hydrogel/silver coatings on in vitro adhesion to catheters of bacteria associated with urinary tract infections.* Curr Microbiol, 2000. **41**(2): p. 120-5.
159. Kamal, G.D., et al., *Reduced intravascular catheter infection by antibiotic bonding. A prospective, randomized, controlled trial.* Jama, 1991. **265**(18): p. 2364-8.
160. Chene, G., G. Boulard, and J.P. Gachie, *[A controlled trial of a new material for coating urinary catheters].* Agressologie, 1990. **31**(8 Spec No): p. 499-501.
161. Thibon, P., et al., *Randomized multi-centre trial of the effects of a catheter coated with hydrogel and silver salts on the incidence of hospital-acquired urinary tract infections.* J Hosp Infect, 2000. **45**(2): p. 117-24.
162. van de Belt, H., et al., *Surface roughness, porosity and wettability of gentamicin-loaded bone cements and their antibiotic release.* Biomaterials, 2000. **21**(19): p. 1981-7.
163. Situ, H. and L.A. Bobek, *In vitro assessment of antifungal therapeutic potential of salivary histatin-5, two variants of histatin-5, and salivary mucin (MUC7) domain 1.* Antimicrob Agents Chemother, 2000. **44**(6): p. 1485-93.
164. Faber, C., et al., *Release of antimicrobial peptide Dhvar-5 from polymethylmethacrylate beads.* J Antimicrob Chemother, 2003. **51**(6): p. 1359-64.
165. Gahr, M., et al., *Influence of lactoferrin on the function of human polymorphonuclear leukocytes and monocytes.* J Leukoc Biol, 1991. **49**(5): p. 427-33.
166. Hwang, P.M., et al., *Three-dimensional solution structure of lactoferricin B, an antimicrobial peptide derived from bovine lactoferrin.* Biochemistry, 1998. **37**(12): p. 4288-98.
167. Mattsby-Baltzer, I., et al., *Lactoferrin or a fragment thereof inhibits the endotoxin-induced interleukin-6 response in human monocytic cells.* Pediatr Res, 1996. **40**(2): p. 257-62.
168. Shau, H., A. Kim, and S.H. Golub, *Modulation of natural killer and lymphokine-activated killer cell cytotoxicity by lactoferrin.* J Leukoc Biol, 1992. **51**(4): p. 343-9.
169. Friedrich, C.L., et al., *Antibacterial action of structurally diverse cationic peptides on gram-positive bacteria.* Antimicrob Agents Chemother, 2000. **44**(8): p. 2086-92.

170. Rodrigues, L., et al., *Strategies for the prevention of microbial biofilm formation on silicone rubber voice prostheses.* J Biomed Mater Res B Appl Biomater, 2007. **81**(2): p. 358-70.
171. Wilcox, S., *The New Antimicrobials: Cationic Peptides.* BioTech Journal, 2004. **2**: p. 88-91.
172. Hancock, R.E.W., *Peptide antibiotics.* The Lancet, 1997. **349**(9049): p. 418-422.
173. Selsted, M.E., et al., *Primary structures of three human neutrophil defensins.* J Clin Invest, 1985. **76**(4): p. 1436-9.
174. Haynie, S.L., G.A. Crum, and B.A. Doele, *Antimicrobial activities of amphiphilic peptides covalently bonded to a water-insoluble resin.* Antimicrob Agents Chemother, 1995. **39**(2): p. 301-7.
175. Adlerova, L., A. Bartoskova, and M. Faldyna, *Lactoferrin: a review.* Veterinarni Medicina, 2008. **53**(9): p. 457–468
176. Bellamy, W., et al., *Antibacterial spectrum of lactoferricin B, a potent bactericidal peptide derived from the N-terminal region of bovine lactoferrin.* J Appl Bacteriol, 1992. **73**(6): p. 472-9.
177. Bellamy, W., et al., *Killing of Candida albicans by lactoferricin B, a potent antimicrobial peptide derived from the N-terminal region of bovine lactoferrin.* Med Microbiol Immunol, 1993. **182**(2): p. 97-105.
178. Gordon, N., et al., *Synthesis and characterization of silver-nanoparticle-impregnated fiberglass and utility in water disinfection.* Nanotechnology, 2009. **20**(49): p. 495705.
179. Levay, P.F. and M. Viljoen, *Lactoferrin: a general review.* Haematologica, 1995. **80**(3): p. 252-67.
180. Sinha, M., et al., *Antimicrobial Lactoferrin Peptides: The Hidden Players in the Protective Function of a Multifunctional Protein.* International Journal of Peptides, 2013. **2013**: p. 12.
181. Svenson, J., et al., *Metabolic fate of lactoferricin-based antimicrobial peptides: effect of truncation and incorporation of amino acid analogs on the in vitro metabolic stability.* J Pharmacol Exp Ther, 2010. **332**(3): p. 1032-9.
182. Groenink, J., et al., *Cationic amphipathic peptides, derived from bovine and human lactoferrins, with antimicrobial activity against oral pathogens.* FEMS Microbiology Letters, 1999. **179**(2): p. 217-222.
183. Nikawa, H., et al., *Fungicidal effect of three new synthetic cationic peptides against Candida albicans.* Oral Dis, 2004. **10**(4): p. 221-8.
184. Ruiz-Gimenez, P., et al., *Antihypertensive properties of lactoferricin B-derived peptides.* J Agric Food Chem, 2010. **58**(11): p. 6721-7.
185. Berman, H.M., et al., *The Protein Data Bank.* Nucleic Acids Res, 2000. **28**(1): p. 235-42.
186. Tomita, M., et al., *Twenty-five years of research on bovine lactoferrin applications.* Biochimie, 2009. **91**(1): p. 52-57.
187. Colas, A. and J. Curtis, *Silicone biomaterials: history and chemistry & medical applications of silicones*, in *Biomaterials Science: An Introduction to Materials in Medicine*, J.E. Lemons, Editor. 2004, Elsevier Amsterdam. p. 80-86.
188. Ren, X., et al., *Electroosmotic properties of microfluidic channels composed of poly(dimethylsiloxane).* Journal of Chromatography B: Biomedical Sciences and Applications, 2001. **762**(2): p. 117-125.

189. Roth, J., et al., *Surface functionalization of silicone rubber for permanent adhesion improvement.* Langmuir, 2008. **24**(21): p. 12603-11.
190. Zhou, J., et al. *One-step surface modification of poly(dimethylsiloxane) by undecylenic acid*. 2008.
191. Mata, A., A.J. Fleischman, and S. Roy, *Characterization of polydimethylsiloxane (PDMS) properties for biomedical micro/nanosystems.* Biomed Microdevices, 2005. **7**(4): p. 281-93.
192. van Poll, M.L., et al., *A Self-Assembly Approach to Chemical Micropatterning of Poly(dimethylsiloxane).* Angewandte Chemie International Edition, 2007. **46**(35): p. 6634-6637.
193. Wong, I. and C.-M. Ho, *Surface molecular property modifications for poly(dimethylsiloxane) (PDMS) based microfluidic devices.* Microfluidics and Nanofluidics, 2009. **7**(3): p. 291-306.
194. Zhou, J., A.V. Ellis, and N.H. Voelcker, *Recent developments in PDMS surface modification for microfluidic devices.* Electrophoresis, 2010. **31**(1): p. 2-16.
195. Makamba, H., et al., *Surface modification of poly(dimethylsiloxane) microchannels.* ELECTROPHORESIS, 2003. **24**(21): p. 3607-3619.
196. McDonald, J.C., et al., *Fabrication of microfluidic systems in poly(dimethylsiloxane).* Electrophoresis, 2000. **21**(1): p. 27-40.
197. Bodas, D. and C. Khan-Malek, *Hydrophilization and hydrophobic recovery of PDMS by oxygen plasma and chemical treatment—An SEM investigation.* Sensors and Actuators B: Chemical, 2007. **123**(1): p. 368-373.
198. Hillborg, H., et al., *Crosslinked polydimethylsiloxane exposed to oxygen plasma studied by neutron reflectometry and other surface specific techniques.* Polymer, 2000. **41**(18): p. 6851-6863.
199. Hillborg, H. and U.W. Gedde, *Hydrophobicity recovery of polydimethylsiloxane after exposure to corona discharges.* Polymer, 1998. **39**(10): p. 1991-1998.
200. Vickers, J.A., M.M. Caulum, and C.S. Henry, *Generation of hydrophilic poly(dimethylsiloxane) for high-performance microchip electrophoresis.* Anal Chem, 2006. **78**(21): p. 7446-52.
201. Dente, S.V., et al., *Malodor neutralizing compositions comprising undecylenic acid or citric acid*. 2013, Google Patents.
202. Hermanson, G.T., *Chapter 13 - Silane Coupling Agents*, in *Bioconjugate Techniques (Third edition)*, G.T. Hermanson, Editor. 2013, Academic Press: Boston. p. 535-548.
203. Wang, L., et al., *Fluorescent Nanoparticles for Multiplexed Bacteria Monitoring.* Bioconjugate Chemistry, 2007. **18**(2): p. 297-301.
204. Hermanson, G.T., *Chapter 3 - Zero-Length Crosslinkers*, in *Bioconjugate Techniques (Second Edition)*, G.T. Hermanson, Editor. 2008, Academic Press: New York. p. 213-233.
205. Claxton, N.S., T.J. Fellers, and M.W. Davidson, *Laser scanning confocal microscopy.* Department of Optical Microscopy and Digital Imaging, Florida State University, Tallahassee, http://www.olympusconfocal. com/theory/LSCMIntro. pdf, 2006.
206. Paddock, S.W., *Confocal laser scanning microscopy.* Biotechniques, 1999. **27**: p. 992-1007.

207. Semwogerere, D. and E.R. Weeks, *Confocal microscopy.* Encyclopedia of Biomaterials and Biomedical Engineering, 2005: p. 1-10.
208. Kaplan, J.B., et al., *Enzymatic detachment of Staphylococcus epidermidis biofilms.* Antimicrob Agents Chemother, 2004. **48**(7): p. 2633-6.
209. O'Gara, J.P. and H. Humphreys, *Staphylococcus epidermidis biofilms: importance and implications.* J Med Microbiol, 2001. **50**(7): p. 582-7.
210. Driscoll, J., S. Brody, and M. Kollef, *The Epidemiology, Pathogenesis and Treatment of Pseudomonas aeruginosa Infections.* Drugs, 2007. **67**(3): p. 351-368.
211. Roy-Burman, A., et al., *Type III Protein Secretion Is Associated with Death in Lower Respiratory and Systemic Pseudomonas aeruginosa Infections.* Journal of Infectious Diseases, 2001. **183**(12): p. 1767-1774.
212. Van Delden, C. and B.H. Iglewski, *Cell-to-cell signaling and Pseudomonas aeruginosa infections.* Emerg Infect Dis, 1998. **4**(4): p. 551-60.
213. Colthup, N.B., L.H. Daly, and S.E. Wiberley, *Introduction to Infrared and Raman Spectroscopy*. 3rd ed. 1990: Academic Press, Inc.
214. Kong, J. and S. Yu, *Fourier transform infrared spectroscopic analysis of protein secondary structures.* Acta Biochim Biophys Sin, 2007. **39**(8): p. 549-59.
215. Urban, M.W., *Vibrational spectroscopy of molecules and macromolecules on surfaces*. 1993, New York John Wiley & Sons, Inc.
216. Bodas, D. and C. Khan-Malek, *Formation of more stable hydrophilic surfaces of PDMS by plasma and chemical treatments.* Microelectronic Engineering, 2006. **83**(4–9): p. 1277-1279.
217. Tian, R., et al., *Infrared Characterization of Interfacial Si−O Bond Formation on Silanized Flat SiO2/Si Surfaces.* Langmuir, 2010. **26**(7): p. 4563-4566.
218. Groenink, J., et al., *Cationic amphipathic peptides, derived from bovine and human lactoferrins, with antimicrobial activity against oral pathogens.* FEMS Microbiol Lett, 1999. **179**(2): p. 217-22.
219. Ruiz-Giménez, P., et al., *Antihypertensive Properties of Lactoferricin B-Derived Peptides.* Journal of Agricultural and Food Chemistry, 2010. **58**(11): p. 6721-6727.
220. Tomita, M., et al., *A review: The active peptide of lactoferrin.* Pediatrics International, 1994. **36**(5): p. 585-591.
221. Hilpert, K., et al., *Screening and characterization of surface-tethered cationic peptides for antimicrobial activity.* Chem Biol, 2009. **16**(1): p. 58-69.
222. Strøm, M.B., J.S. Svendsen, and Ø. Rekdal, *Antibacterial activity of 15-residue lactoferricin derivatives.* The Journal of Peptide Research, 2000. **56**(5): p. 265-274.
223. Bellamy, W., et al., *Killing of Candida albicans by lactoferricin B, a potent antimicrobial peptide derived from the N-terminal region of bovine lactoferrin.* Medical Microbiology and Immunology, 1993. **182**(2): p. 97-105.
224. Kang, J.H., et al., *Structure–biological activity relationships of 11-residue highly basic peptide segment of bovine lactoferrin.* International journal of peptide and protein research, 1996. **48**(4): p. 357-363.
225. Yamauchi, K., et al., *Antibacterial activity of lactoferrin and a pepsin-derived lactoferrin peptide fragment.* Infect Immun, 1993. **61**(2): p. 719-28.

226. Ulvatne, H., et al., *Lactoferricin B inhibits bacterial macromolecular synthesis in Escherichia coli and Bacillus subtilis.* FEMS Microbiol Lett, 2004. **237**(2): p. 377-84.
227. Kabara, J.J., et al., *Fatty acids and derivatives as antimicrobial agents.* Antimicrob Agents Chemother, 1972. **2**(1): p. 23-8.
228. Kull, F.C., et al., *Mixturs of quaternary ammonium compounds and long-chain fatty acids as antifungal agents.* Appl Microbiol, 1961. **9**: p. 538-41.
229. Li, X.C., et al., *Potent in vitro antifungal activities of naturally occurring acetylenic acids.* Antimicrob Agents Chemother, 2008. **52**(7): p. 2442-8.
230. Owen, M.J. and P.J. Smith, *Plasma treatment of polydimethylsiloxane.* Journal of Adhesion Science and Technology, 1994. **8**(10): p. 1063-1075.